



BRNO UNIVERSITY OF TECHNOLOGY

VYSOKÉ UČENÍ TECHNICKÉ V BRNĚ

FACULTY OF MECHANICAL ENGINEERING

FAKULTA STROJNÍHO INŽENÝRSTVÍ

INSTITUTE OF AEROSPACE ENGINEERING

LETECKÝ ÚSTAV

WIND TUNNEL MEASURING EQUIPMENT CALIBRATION

KALIBRACE MĚŘICÍHO ZAŘÍZENÍ AERODYNAMICKÉHO TUNELU VUT

MASTER'S THESIS

DIPLOMOVÁ PRÁCE

AUTHOR

AUTOR PRÁCE

BSc Hendrik de Boer

SUPERVISOR

VEDOUCÍ PRÁCE

Ing. Jiří Matějů

BRNO 2021

Specification Master's Thesis

Department: Institute of Aerospace Engineering
Student: **BSc. Hendrik de Boer**
Study program: Mechanical Engineering
Study Branch: Aircraft Design
Supervisor: Ing. Jiří Matějů
Academic year: 2020/2021

Pursuant to Act no. 111/1998 concerning universities and the BUT study and examination rules, you have been assigned the following topic by the institute director Master's Thesis:

Wind tunnel measuring equipment calibration

Concise characteristic of the task:

A lot of experimental equipment for a wind tunnel experiment is placed at the Institute of Aerospace Engineering. For accurate experimental results, calibration is necessary according to the proper method and at given time intervals. Calibration is a time-consuming process without additional information about the experiment. This is the reason the optimization of the process of calibration will be useful for more effective work with the wind tunnel.

Goals Master's Thesis:

Literature review of the calibration process for chosen equipment.

Programming of calibration procedures.

Calibration procedures report.

Calibration sheets.

Recommended bibliography:

BARLOW, Jewel B.; RAE, William H.; POPE, Alan. Low-speed wind tunnel testing. John Wiley & Sons, 1999.

Deadline for submission Master's Thesis is given by the Schedule of the Academic year 2020/21

In Brno,

Signatures

Abstract

In this thesis the topic of calibration of devices and sections has been investigated in relation to the wind tunnel at the Brno Institute of Aerospace Engineering. The instruments used in the wind tunnel are calibrated and section calibrations on the test section are described and performed. Calibration sheets and report templates are made to simplify future processes. The newly calibrated set-up is used to perform force and wake measurements on a model car, which are compared to measurements pre-calibration to further exemplify the usefulness of calibrations.

Key words

Instrument calibrations, Test section calibrations, Wind tunnel, aerodynamics, wake measurement

DE BOER, Hendrik. *Wind tunnel measuring equipment calibration*. Brno, 2021. Available also at: <https://www.vutbr.cz/studenti/zav-prace/detail/132710>. Master's Thesis. Vysoké učení technické v Brně, Fakulta strojního inženýrství, Institute of Aerospace Engineering. Supervisor Jiří Matějů.

I hereby declare that I am the sole author of this master's theses and that I have not used any sources other than those listed in the bibliography and identified as references. I further declare that I have not submitted this thesis at any other institution in order to obtain a degree.

BSc. Hendrik de Boer

Acknowledgements

I would like to thank everyone that made it possible for me to finish this work. That includes professors who got me ready for this in previous courses, university staff that went out of their way to make it possible for me to even go to university in the lockdown era, and of course my supervisor Jiří Matějů who spent countless hours patiently helping all along the way.

Contents

Contents.....	7
1 Introduction	11
1.1 Wind tunnel	12
1.1.1 Conditioning chamber	13
1.1.2 Test section.....	14
2 Calibrations	15
2.1 Devices	16
2.2 Calibration Sheets.....	18
2.2.1 Pressure transducer calibration.....	21
2.2.2 Temperature sensors.....	26
2.2.3 Force sensor.....	28
2.3 Section Calibrations.....	29
2.3.1 Uniformity of flow in the test section	30
2.3.2 Dynamic pressure gradient.....	32
2.3.3 Flow angularity	37
2.3.4 Large scale fluctuations.....	38
3 Calibration report	44
4 Test measurement.....	45
4.1 Model.....	45
4.2 Force measurement device	46
4.3 Load and wake measurements	49
5 Evaluation.....	53
6 Conclusion.....	54
Bibliography.....	55
Nomenclature	56
Appendix A	57

Characteristics of thesis dilemma (stated on vut.br/studis):

A lot of experimental equipment for a wind tunnel experiment is placed at the Institute of Aerospace Engineering. For accurate experimental results, calibration is necessary according to the proper method and at given time intervals. Calibration is a time-consuming process without additional information about the experiment. This is the reason the optimization of the process of calibration will be useful for more effective work with the wind tunnel.

Objectives which should be achieved:

Literature review of the calibration process for chosen equipment.

Programming of calibration procedures.

Calibration procedures report.

Calibration sheets.

1 Introduction

In this thesis the topic of calibration of devices is investigated in relation to the wind tunnel at the Brno Institute of Aerospace Engineering. Calibrations can be seen as a verification or readjustment of a device or section and should be done on a regular base to confirm reliability of the results. They can be divided into two groups, device calibrations and section calibrations. The current measurement devices are tested and if needed recalibrated. Following that the test section of the wind tunnel is investigated, where the air streams and conditions of an empty wind tunnel are closely mapped following calibration methods of wind tunnels described by Barlow Rae and Pope (1999) [1].

Calibration sheets and reports are made to streamline the calibration process, as well as to facilitate a quick browse of the conditions of the wind tunnel and its devices.

Lastly the calibrated devices and section are used in an experiment to determine the drag constant of a model car. The results are compared to results without calibrated conditions to determine the usefulness of the calibrations.

1.1 Wind tunnel

The Brno Institute of Aerospace Engineering operates a closed loop wind tunnel, for which a schematic can be seen in Figure 1.

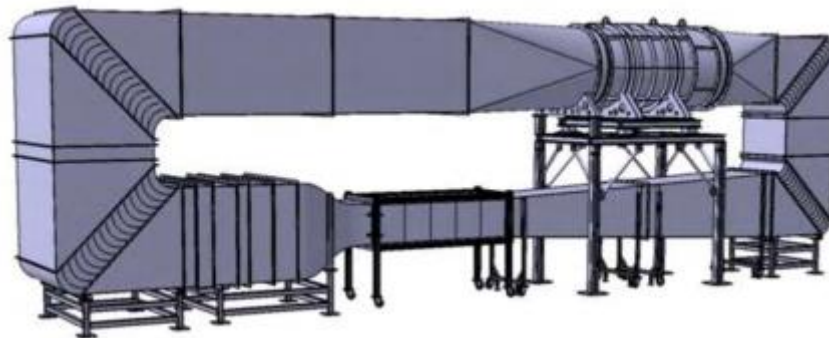


FIGURE 1: SCHEMATIC OF THE MAIN WIND TUNNEL OF THE BRNO IAE [10]

The closed loop system provides some advantages over the open wind tunnel counterpart, mentioned in *Low-Speed Wind Tunnel Testing* by Barlow, Rae and Pope [1]

1. less interaction with environment
2. more controllable quality of the flow
3. less energy is required

That there is less interaction with the environment can be derived from the name, a closed loop wind tunnel. In general the air in the wind tunnel stays inside, the only interaction with the outside world being through the walls.

Point 2 follows from the first, as air flow outside the closed loop tunnel does not affect the flow within, like it would for an open set up. That does not mean however that the environment has no effect at all on the quality of flow. Outside temperatures and air pressure still affects the air within the wind tunnel, but effect is more gradual and measureable, and can thus be accounted for in measurement results.

Not having to constantly accelerate air from 0 m/s to the test velocity, but instead keeping a constant flow throughout the tunnel reduces the required energy from the turbine. The energy consumed is not a priority for the measurements themselves, but can be assumed to be an important factor for the Institute of Aerospace Engineering.

Barlow Rae and Pope [1] also names some disadvantages, namely;

1. There must be a way to purge the tunnel
2. Air exchanger or cooling method is necessary
3. The initial cost is higher

The first point is to say that if anything is set loose in the wind tunnel it will keep going around, unless filtered out. This can be related to smoke used in visualization experiments, or fluids used for particle image velocimetry, PIV [5]. Next to intended additions to the system there is also the case in which the model or part of the model comes loose during

measurements in the test section. This kind of debris should be stopped and filtered out immediately before damaging the wind tunnel from within.

As for the air within the closed loop, an increasing temperature over time can be expected from the energy added to the closed system by the turbine. The increased temperature affects the air density, which in turn affects the speed of flow in the tunnel. Either the system should be cooled to keep a constant temperature, or extra work needs to be done to adjust measurement results. For cooling there are generally two options mentioned, either cooling through the walls and corner vanes, or through a radiator in the settling chamber [15].

Lastly the initial costs of construction of the closed loop wind tunnel are higher due to extra required parts, like the cooling system mentioned above, or the corner vanes used to direct the flow around the loop.

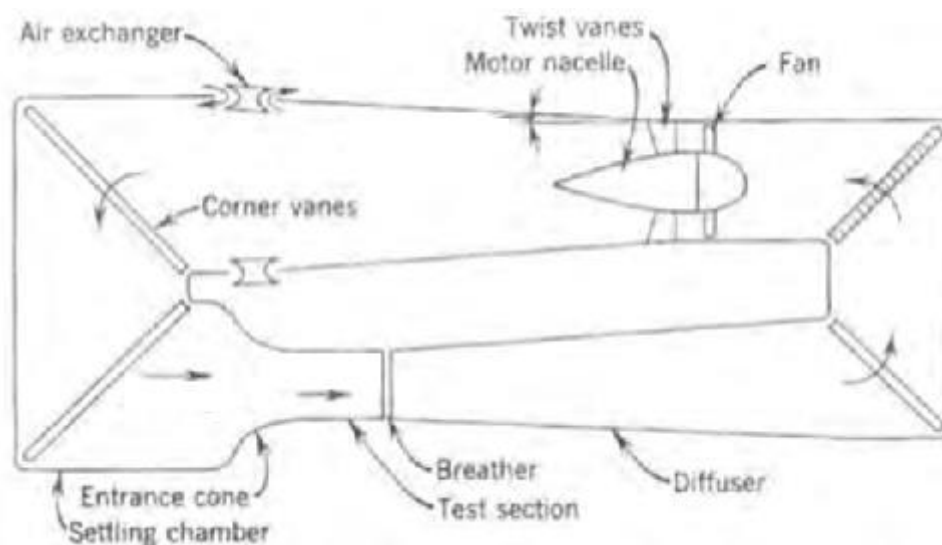


FIGURE 2: NOMENCLATURE WIND TUNNEL

In Figure 2 a schematic of the wind tunnel is shown. The positions of the different parts, and sizes of the sections do not exactly mimic the real wind tunnel at the Institute of Aerospace Engineering, though the general idea is the same. The fan, or turbine in the top right accelerates air counterclockwise, which in the corners gets redirected by the corner vanes. The conditioning chamber in the bottom left prepares the air for the test section, where the air flow should be steady for accurate measurements. After the test section the flow gets through the diffuser, directed back through the corners to the turbine.

1.1.1 Conditioning chamber

The conditioning chamber or settling chamber is the last area before the test section. It contains hexagonal shaped grid along the cross-sectional area right after the corner vanes, to redirect the flow in a straight path, reducing the angular momentum the air gained from going through the two corners. The radiator tubes are situated there as well to keep the temperature in the wind tunnel stable. Right after the cross-sectional area is greatly reduced by the entrance cone, to increase the free stream velocity into the test section.

The conditioning chamber at the Brno institute of Aerospace Engineering contains one pressure sensor for the static pressure, as well as a Pitot tube right after the entrance cone to measure the dynamic pressure of the flow entering the test section. Two thermocouples are present to measure the free flow temperature.

1.1.2 Test section

The test section of the wind tunnel consists of 20 glass panels, 5 per side that together make a 2 meter, 700mm wide by 500mm high rectangular section. A few wall sections contain small holes to let in the support and wiring for the models and measurement equipment. All the section walls are replaceable which gives freedom of where to place models and where to measure the flow.



FIGURE 3: TEST SECTION SCHEMATIC. [10]

Close to half way the section length the Traver system can be found, which is a programmable robot-arm. It carries a Pitot tube and Kiel tube, which can be moved anywhere along the cross-sectional area.

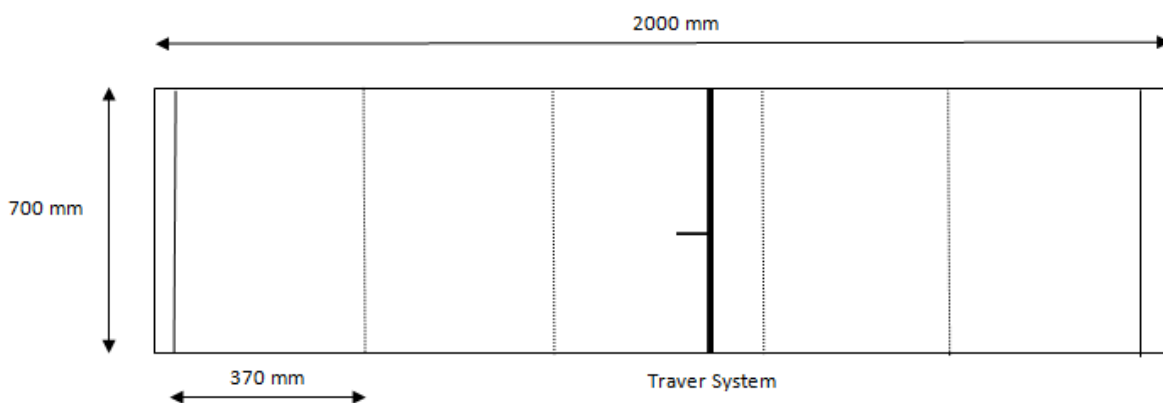


FIGURE 4: TEST SECTION TOP VIEW WITH VISIBLE TRAVER SYSTEM

2 Calibrations

Calibrations can be seen as a verification or readjustment of a device and should be done on a regular base to confirm reliability of the results. It can be seen as a maintenance procedure to ensure proper functioning. For this thesis the calibrations are divided into two groups; device calibrations and section calibrations.

Devices:

- Pressure sensors
- Temperature sensors
- Force sensors

Section calibrations:

- Velocity variation in the plane of the model
- Longitudinal dynamic pressure variation
- Flow angularity
- Extend of large-scale fluctuations

Device calibrations should be performed first, as these same devices are later used to perform the section calibrations.

2.1 Devices

The first group, the devices, concerns the measuring equipment. The current performance of the device should be verified using known inputs and expected outputs. This can be done using certain physical properties, or with calibration devices for which the accuracy is known to be high. In case the results are adequate the device can be considered calibrated. If the results are out of tolerance a consideration should be made, whether the device is damaged and needs to be repaired or whether a change of calibration constants is enough to obtain accurate results again. Reparations are costly and time consuming, and should be avoided if possible. Obtaining new calibration constants is a relatively simple process, but can be time consuming. It is done by collecting various known points along the range of the device, after which the calibration constants are adjusted in such a way that the device's output is equal to the desired output. If this is done correctly the device can be considered calibrated. The device should then be labeled with the name and date of the calibration for further use, conforming to ISO 9001 standards for quality measurements, to be sure of the calibration status. Figure 5 shows a simple to follow process map for the use of new or existing devices.

The main instruments used in a wind tunnel are the pressure transducers used to measure the dynamic pressure at a certain point in or before the test section. The wind tunnel also operates three thermocouples to measure the outer temperature and air temperature within the tunnel in order to describe experimental conditions. For this thesis the thermocouples are considered up to standard and will not be calibrated. Similarly, the force transducer has been calibrated last December by an outside source and will not be recalibrated.

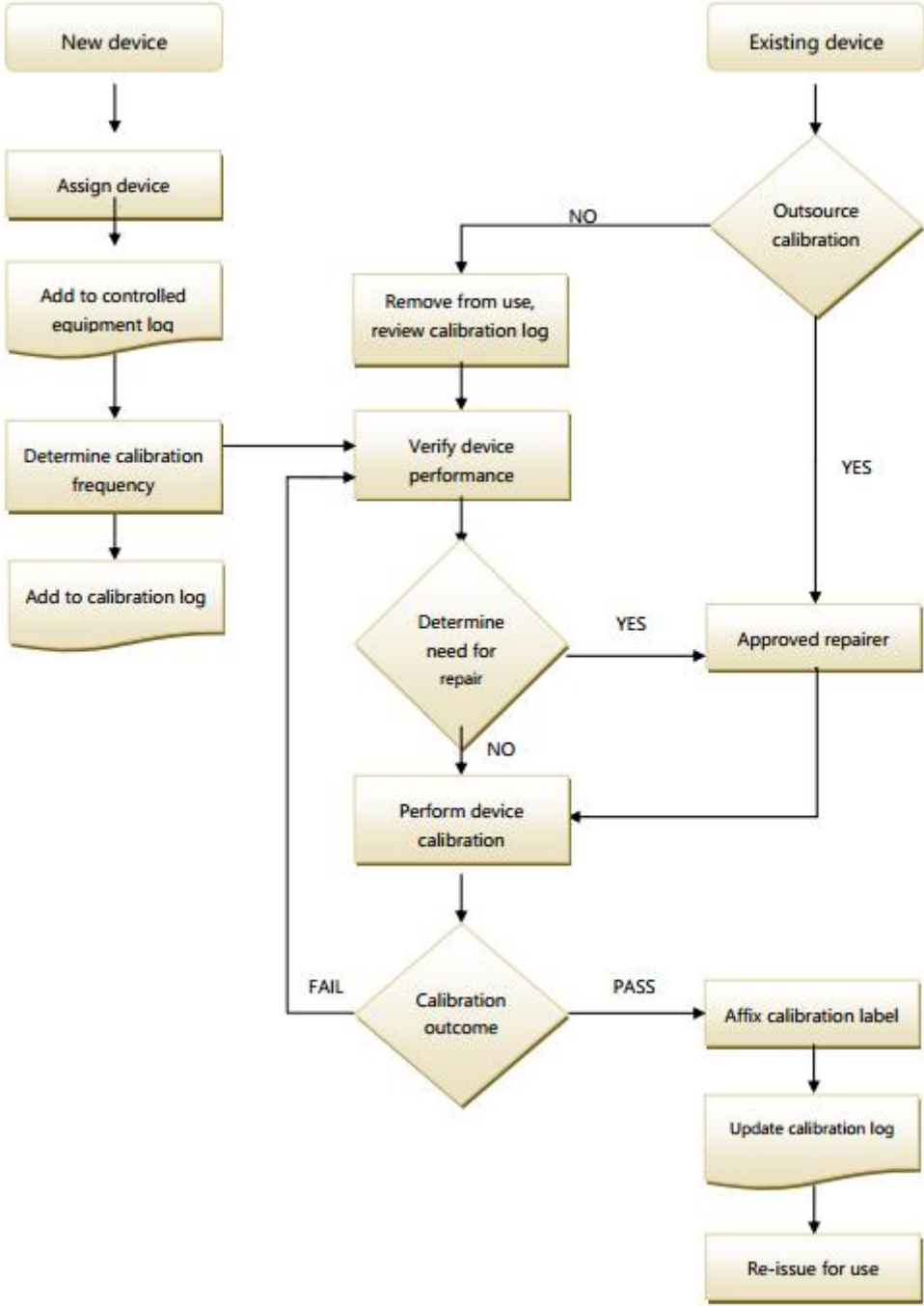


FIGURE 5: ISO 9001 CALIBRATION PROCESS MAP

2.2 Calibration Sheets

Calibration sheets are made to promote clarity and continuity of calibrations. The calibration process can be time consuming, thus a clear overview of when the last calibration has been performed, and what the results were can save a lot of time. After calibration a tag should be created that can be stuck to or near the calibrated device. It should contain a tag/report number, the calibration date and whether the device is qualified for use. The tag number should reference to the calibration report, which should be kept for reference. It could even be possible to use a scan able QR code on the tag to obtain the report from an online source.

Calibration Report			
General			
Tag:		Module:	Pressure
Area:	Wind tunnel IAE	Report Number:	2
Hookup:	1mm PVC tube	Date of Calibration:	14-5-2021
Technician:	Hendrik de Boer	Printed:	
Work Order:	CAL, as found	AmbientTemp:	22,016 C
Cal model Num:	DPI 665	Cal Serial Num:	X187692
Instrument			
model:	PX 655 50D1	Error calculation	difference
serial number:	X12300013	Pass/Fail tolerance	0,5
input:	0-12500 Pa	Output:	4-20 mA
Calibration Data			
Calibration points	Readings	Error %	Status
0		0,006	
50		23,404	53,192 Fail
102		77,1	24,41176471 Fail
200		179,733	10,1335 Fail
<hr/>			
Comments			
current constants	K= 777.44 B = -3098.42	previous results from Jiri Mateju, 2016	
<hr/>			
Date:	14-5-2021	Approved by:	

FIGURE 6: EXAMPLE CALIBRATION SHEET FOR THE CALIBRATION OF A PRESSURE TRANSDUCER

The calibration report is divided into two pages; the first page contains all the necessary information about the device and the measured calibration points. The second page then uses these points to propose a new calibrated line with the accompanying constants.

The first page contains four main areas, the General, Instrument and Calibration Data and the last comments. The general area consists of data about when the calibration was performed, by whom, which device was used to calibrate and what the conditions were.

The instrument section gives more information on the calibrated device. The model, serial number of the particular device and range of the device are shown. The pass/failure rate is determined by the error stated by the manufacturer for said device.

The Calibration data is the main body of the document, of which only a part is shown in Figure 6. The first row contains the points that are investigated, with the second row being the readings from the calibrated device. Assuming perfect readings from the calibrator, in this case the Druck DPI 650, the difference between the calibration point and the reading from the calibrated device, the pressure transducer, can be considered the error for said point. Per point it can then be indicated whether the error is small enough to pass or fail the desired tolerance of the device, and thus whether changes are required.

Lastly, on the bottom of the page room is left for additional comments, as well as space for the date of calibration, and name and signature of the person responsible for the calibrations.

The second page of the Calibration report is automatically constructed using the calibration point inputs and the given input and output ranges. The graph on top of the page shows the calibration points curve in blue. The calculated proposed curve for the transducer is given in green. Below the graph the slope and intercept constants are shown, as well as the correlation coefficient R and the R^2 value, used to indicate the goodness of a fit.

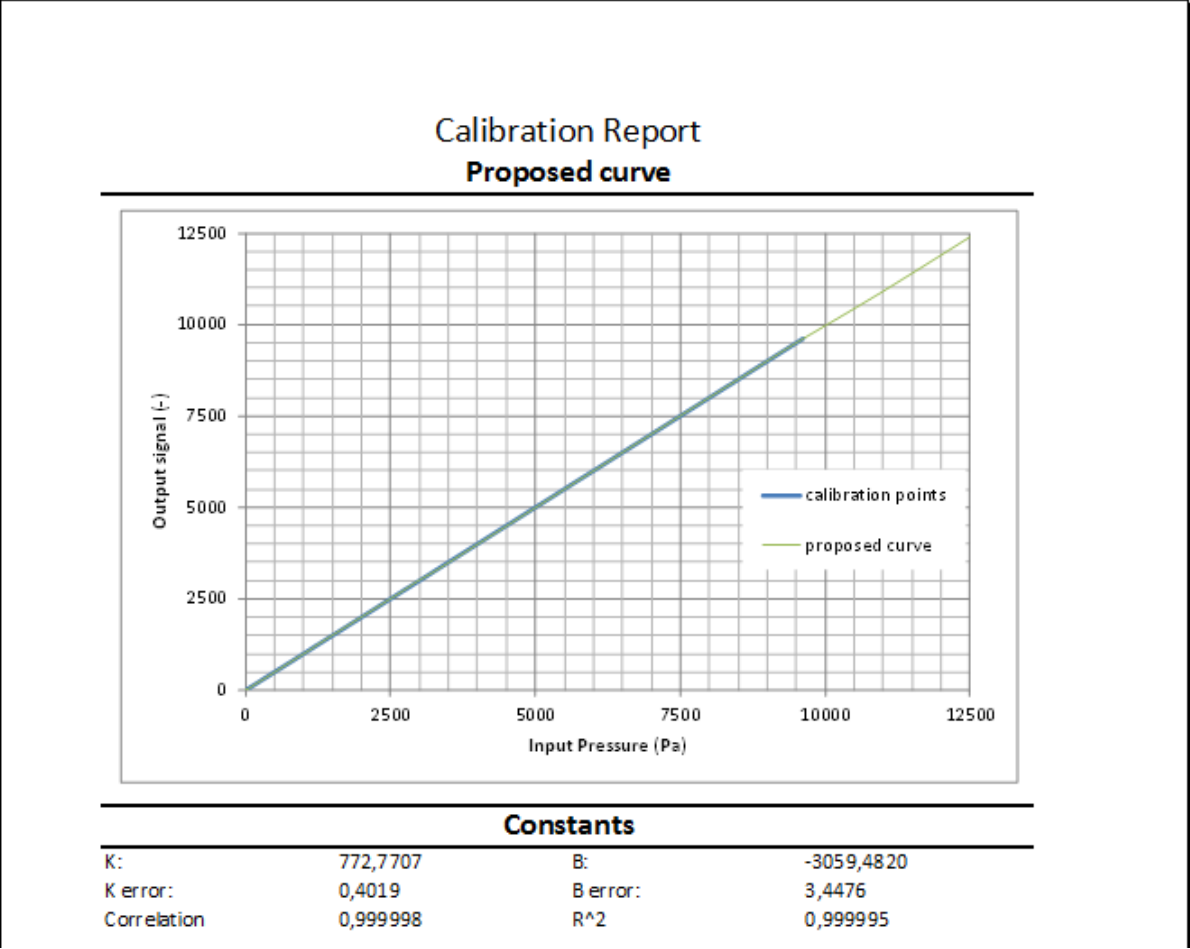


FIGURE 7: SECOND PAGE OF THE CALIBRATION REPORT, SUGGESTED CURVE AND CONSTANTS

2.2.1 Pressure transducer calibration

The pressure transducers at the institute normally work by converting incoming air pressure from a pitot tube to an electrical signal. This signal can then be converted in a visible number which indicates the pressure the transducer measured. There are four different transducers available, each with a different range of pressures (and thus wind tunnel velocities). During wind tunnel measurement two of the four transducers are active, one for the pressure measured in the conditioning chamber and the other for the movable Pitot tube in the test section.

Name	01D1	10D1	25BDI	50D1
Range (Pa)	0-249	0-2490	0-6230	0-12500

The transducers are supposed to have an accuracy of 0.5% of the full scale, and 0.4% full scale non-linearity. Over time the stability can change with $\pm 0.5\%$ FS/year.

Calibration of pressure transducers was performed with a Druck DPI 650, which has an accuracy a 0.05% error when measuring in the range of 7000 Pa, which comes down to an error of 3.5Pa . The device is connected to the transducer with a tube that normally connects the transducer to a Pitot probe. The pressure is gradually increased, for which at various points the displayed pressure on the DPI 650 is compared to the output signal of the pressure transducer. For the output signal the following equations holds, for which P is pressure, I is the signal's current in mA, and K and B are the calibration constants.

$$P = KI + B \quad (1)$$

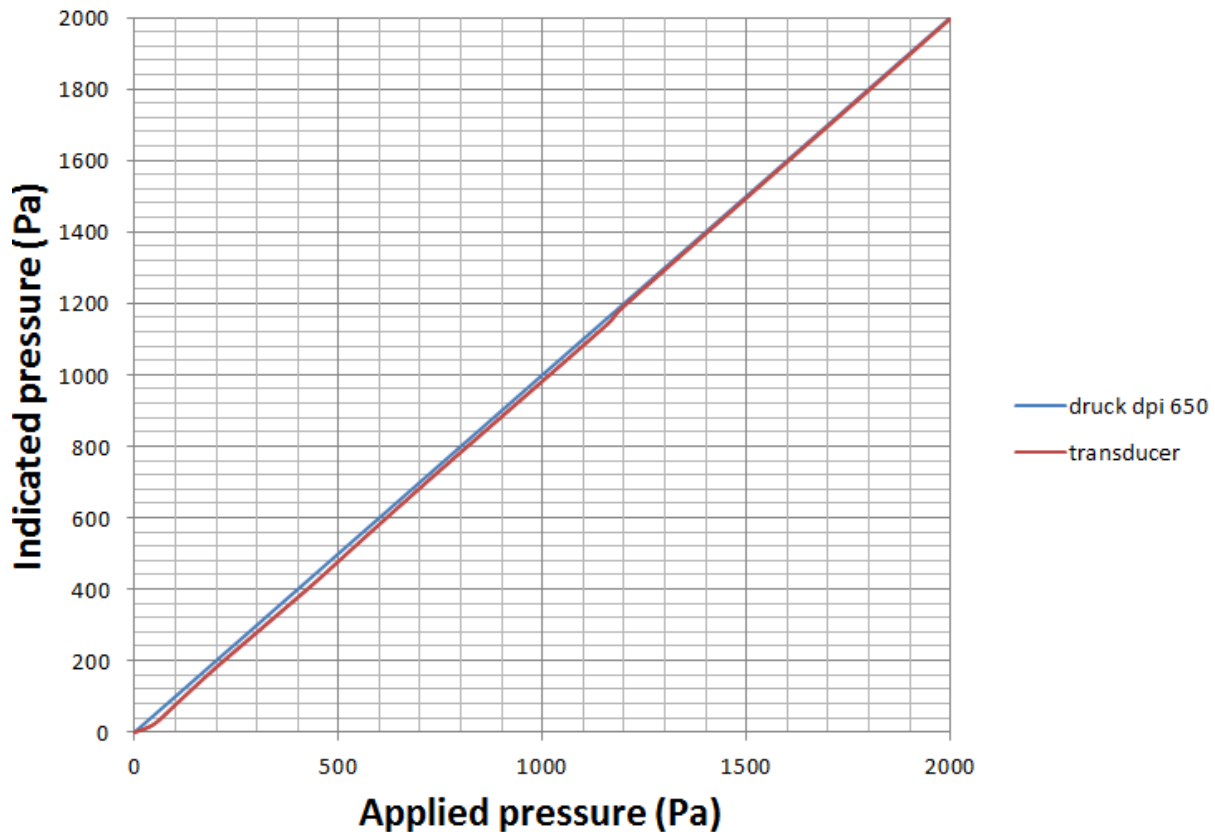


FIGURE 8: APPLIED VS INDICATED PRESSURE

In Figure 8 the indicated dynamic pressure can be seen on the Y axis, with the applied pressure by the Druck device on the X axis. The indicated and applied pressure values are the same for the Druck DPI, but it can be seen that the output from the 50D1 transducer does not overlap. For the lower pressure range the output values are about 20 Pa lower, and above 8000 Pa the error is around 30 Pa. While the result is not perfect, it isn't very far off which leads to believe that the transducer is not broken, and recalibration of the constants will suffice.

Using equation 1 the output current can be found as the old constants K and B are known and the pressure P is read off from the calibrator. Through linear regression the K and B constants are found that will satisfy the desired pressure readouts. First requirements to calculate these are the square distances from the mean for both the amplitude on the x axis and pressure on the y axis.

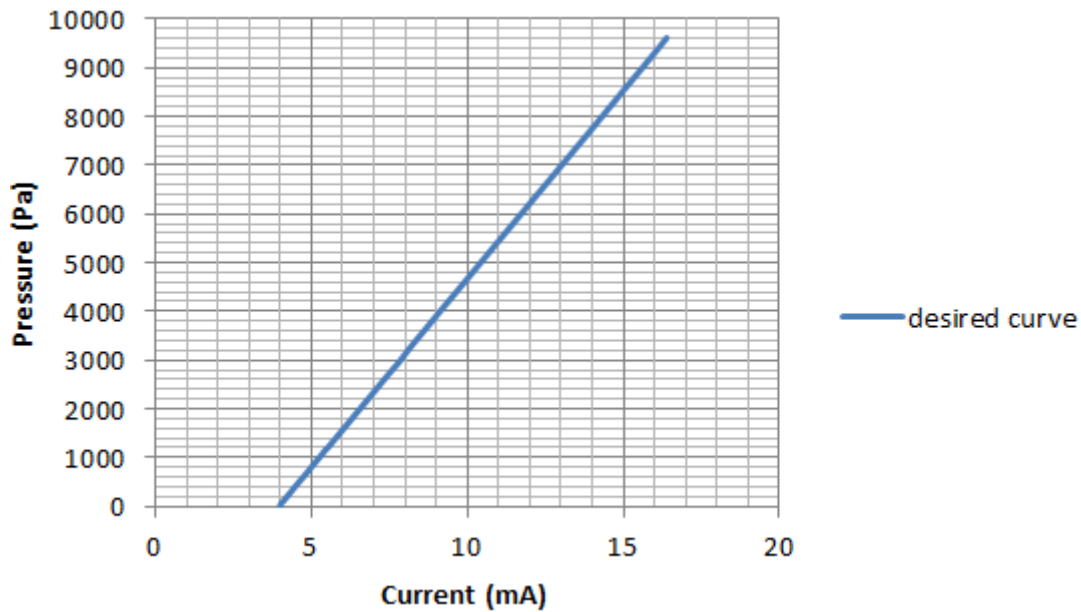


FIGURE 9: PRESSURE READOUTS PLOTTED AGAINST THE OUTPUT CURRENT FROM THE TRANSDUCER

Equations 2.1 and 2.2 show the sum of square errors for both x and y , with equation 2.3 combining the two errors in x and y . x_i and y_i indicate the measured value, where x_m and y_m indicate the respective means of the measurements of x and y .

$$s_{xx} = \sum_{i=1}^n (x_i - x_m)^2 \quad (2.1)$$

$$s_{yy} = \sum_{i=1}^n (y_i - y_m)^2 \quad (2.2)$$

$$s_{xy} = \sum_{i=1}^n (x_i - x_m)(y_i - y_m) \quad (2.3)$$

K is then calculated using the idea that the best fit is where the square distance of all the points to the line is minimal:

$$K = \frac{s_{xy}}{s_{xx}} = 772.771 \frac{Pa}{mA} \quad (2.4)$$

Then the intercept B is:

$$B = y_m - Kx_m = -3098.4 Pa \quad (2.5)$$

For the standard deviation of the slope K and intercept B first the standard deviation of the function $y(x)$ is calculated, also called the residual sum of squares.

$$\sigma_{yx}^2 = \frac{1}{n-2} \sum_1^n (y_i - y_{ei})^2 = 55.16 \tag{2.6}$$

This value by itself does not indicate much, but it can be used to construct confidence intervals and prediction intervals. In this project it is divided by the sum of square errors for x to obtain the standard deviation of the slope K.

$$\sigma_K^2 = \frac{\sigma_{yx}^2}{S_{xx}} = 0.1615 \tag{2.7}$$

As variance can be described as the square root of the standard deviation, it follows that the variance in the slope K is 0.402 Pa/mA.

$$\sigma_B^2 = \sigma_{yx}^2 \left(\frac{1}{n} + \frac{x_m^2}{S_{xx}} \right) = 11.8859 \tag{2.8}$$

This brings the variance in the intercept B to 3.448 Pa.

TABLE 1: CALIBRATION CONSTANTS

	K (Pa/mA)	B (Pa)
Old	777,44	-3098,4
New	772,77071±0,402	-3059,482 ± 3,448

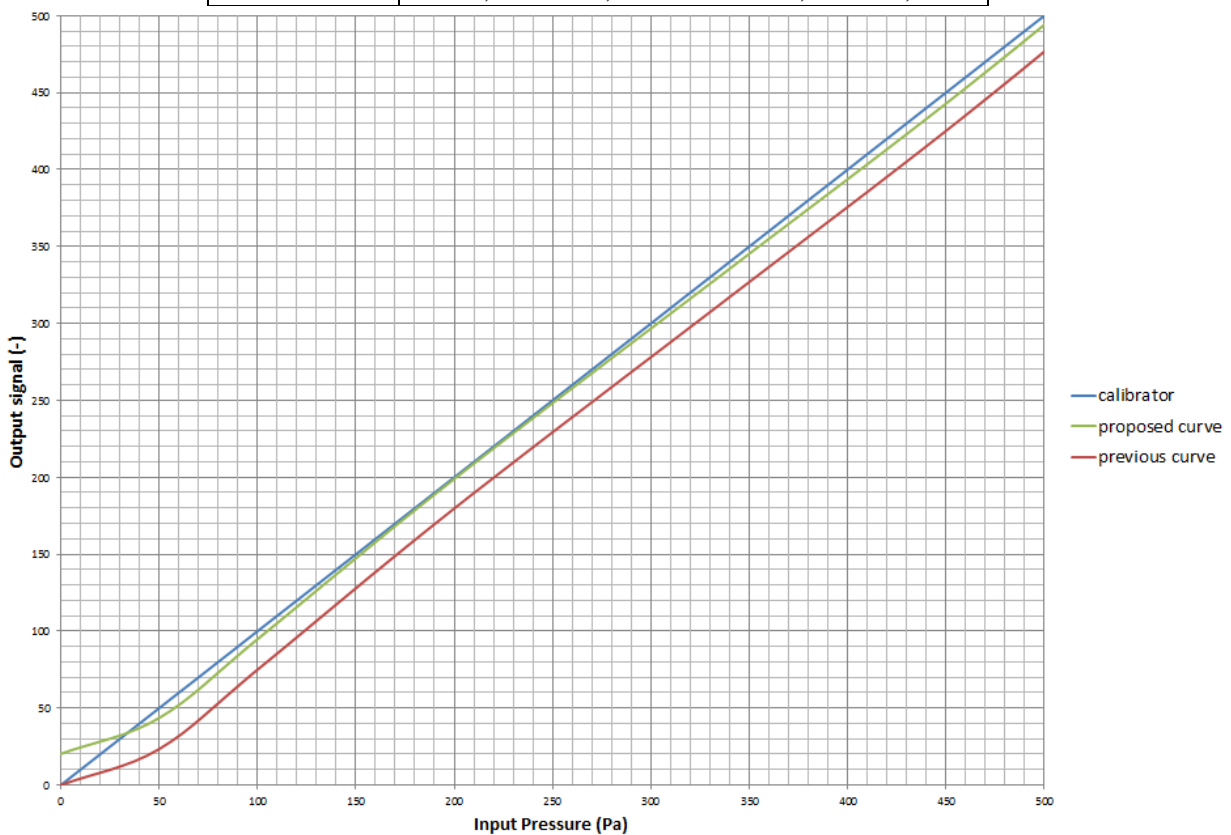


FIGURE 10: TRANSDUCER CURVES

There are various tests to evaluate the proposed linear regression model apart from observing a close fitting curve like in Figure 10. The ones used in this dissertation use the sums of squares as a starting point. The first is the Regression sum of squares, which describes how well a regression model represents the modeled data, with lower values indicating that it does so.

$$Regression_{SS} = \sum_1^n (y_{e_i} - y_m)^2 \quad (2.9)$$

In equation 2.9 y_{e_i} is the estimated value by the regression model and y_m the mean value. The following sum of squares is the residual sum of squares, or the sum of squared errors. It is calculated using the predicted values by the regression and the observed values.

$$Residual_{SS} = \sum_1^n (y_{o_i} - y_{e_i})^2 \quad (2.10)$$

In equation 2.10 y_{o_i} is the observed values for each point i . In general a lower $Residual_{SS}$ indicates that the model is well able to explain the data. The regression and residual sum of squares can be combined to obtain R^2 , the square of the correlation coefficient R .

$$Total_{SS} = \sum_1^n (y_{o_i} - y_m)^2 = Regression_{SS} + Residual_{SS} \quad (2.11)$$

$$R^2 = \frac{Regression_{SS}}{total_{SS}} = 0.999995 \quad (2.12)$$

R^2 being the how well the model can explain variability, with values close to 1 indicating a better fit between the predicted and actual value. In combination with the low variances in the slope coefficient K and intercept B the R^2 value shows that the model fits very close and describes the data points well.

These steps are performed for all 4 transducers, to ensure the quality of the calculated calibration coefficients.

TABLE 2: CALIBRATION CONSTANTS FOR EACH PRESSURE TRANSDUCER

Name	01D1	10D1	25BD1	50D1
Range (Pa)	0-249	0-2490	0-6230	0-12500
K	155,189 ±0,088	155,189 ±0,182	775,269 ± 0,528	772,771 ±0,402
B	86,528 ±0,417	886,565 ±0,831	4803727 ±3272,755	-3059,482 ±3,448
R^2	0,999714	0,999971	0,999991	0,999995

2.2.2 Temperature sensors

The wind tunnel at the Institute of Aerospace technology operates three thermocouples during measurements. The work on the principle of consisting of two different metals with different specific heat values, which are thus differently affected by heating and cooling. This directly affects the voltage in the thermoelectric circuit, which can be correlated back to a temperature.

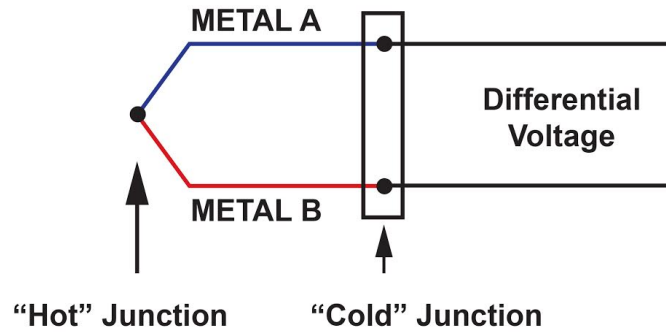


FIGURE 11: SIMPLIFIED THERMOCOUPLE DIAGRAM

Two of these thermocouples measure the air temperature within the wind tunnel, while the third measures the room conditions. Temperature in general will not be the primary measurement result from a wind tunnel experiment; however temperature measurements are important for accurate condition determination. In equation 2.13 the relation between temperature, static pressure and density is shown, with R being the air gas constant 287.058 J/Kg K.

$$\rho = \frac{P}{RT} \quad (2.13)$$

The wind tunnel computer system automatically calculates the density of the air within the tunnel from an average between the inner temperature and the room temperature. This density is then used to calculate the free flow velocity together with the dynamic pressure, seen in equation 2.14.

$$V = \sqrt{\frac{2 \cdot p_d}{\rho}} \quad (2.14)$$

From the above it follows that the temperature measurements ensure both the conditions of the experiment as well as the direct measurement results. Therefore it is important to work with calibrated thermocouples to ensure well defined and accurate results.

Calibrations can be performed in a number of ways, though the principle remains the same. The thermocouple is used to measure known temperatures, for instance a known fixed temperature point like the boiling or freezing point of certain substances. Another option is to compare the thermocouple results to that of an accurate, calibration thermocouple. In case the thermocouple gives the same results as expected it can be considered calibrated. If the results differ the calibration constants should be altered, in a similar way as has been done for

the pressure transducers in the previous chapter. The thermocouples for the wind tunnel had been recently calibrated and are considered up to standards, therefore recalibration is unnecessary.

2.2.3 Force sensor

Force transducers work on the principle of inner strain gauges and spring elements. When force is applied to the sensor the inner strain gauges stretch out or contract, which in turn increases or decreases the electrical resistance. This allows for the measurement of the current, which then gives a description of the applied force. The sensor used in the institute's wind tunnel, an Ati mini 40-a is able to recognize forces in 6 degrees of freedom, for all possible translations and rotations. Its calibration has recently been outsourced to a qualified company, and its measurements are considered up to standards. The calibration sheets can be found in appendix A. For the ranges and errors of the sensor the guidelines from the producer are followed.

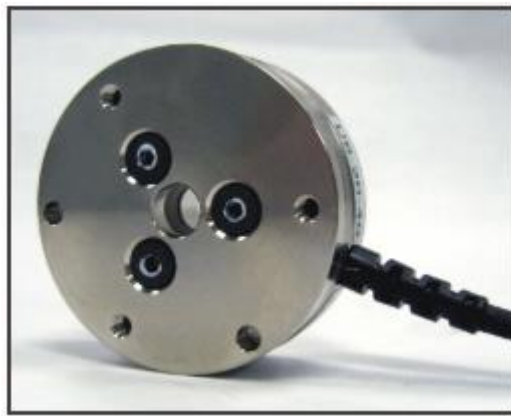


FIGURE 12: ATI MINI 40-A

TABLE 3: SENSING RANGE OPTIONS FOR THE SENSOR

Calibration	F _x (N)	F _y (N)	F _z (N)	T _x (Nm)	T _y (Nm)	T _z (Nm)	F _x (N)	F _y (N)	F _z (N)	T _x (Nm)	T _y (Nm)	T _z (Nm)
Si-20-1	20	20	60	1	1	1	0.25	0.2	0.45	0.0125	0.0125	0.02
Si-40-1	40	40	120	2	2	2	0.5	0.4	0.9	0.025	0.025	0.04
Si-80-1	80	80	240	4	4	4	1	0.8	1.8	0.05	0.05	0.08
Sensing ranges							Error					

Table 3 shows the ranges and errors of the sensor. Three calibration options are given, with accompanying sensing ranges and errors. For all the measurements in this thesis the most course calibration, Si-80-1, is used due to the higher sensing range.

2.3 Section Calibrations

For the reliability of the measurement results more should be done than just the calibration of measurement devices. In general wind tunnel measurements are performed by inserting a model into the test section, and then determining the flow around this model in some way. These results only hold any significance when the original flow, without the model, is carefully described. Therefore section calibrations should be performed; to obtain a clear indication of the free flow through the test section.

AGARDograph 54 [13] summarizes the calibration techniques used for low-speed wind tunnels, which the one at the Institute of Aerospace Engineering can be considered. The document mentions the following results that should be obtained before calling the wind tunnel calibrated:

- Velocity variation in the plane of the model
- Longitudinal dynamic pressure variation
- Extend of large-scale fluctuations
- Flow angularity

Obtaining results for the above allows the user to describe the free flow velocity in the test section; along the length and cross sectional area where the model will be placed, so that any changes in the flow that occur from the presence of the model are noticeable. In this thesis the flow angularity calibration had to be canceled, due to the unusable state of the 5-hole probe that is required for the measurements.

2.3.1 Uniformity of flow in the test section

Preferably the free flow velocity is uniform all over the test section cross-section, however in general a difference can be seen along the walls and in the corners. Air flow close to the test section walls creates a boundary layer, for which the flow velocities differ from the free flow velocity. The flow velocity at the wall will be close to 0, gradually increasing over the distance between the measuring point and the wall. This effect can be expected to be even more pronounced in the corners, due to having the flow velocity differences due to two boundary layers close by.

Using the traverse system, a Pitot tube is moved along a grid of measurement points on the cross-section of the test section. The cross section that is measured is at the same distance into the test section as common dynamic pressure measurements in the wind tunnel, which is 755mm into the test section. The grid is 12 points by 12 points, 440mm in height and 660 mm in width. The height and width of the grid were chosen in a way to get as close to the test section walls without causing any damage. At each point 10 measurements take place, 0.3 seconds after each other. The results are averaged to obtain the average dynamic pressure for that point. The velocity V for the point is derived from the measured dynamic pressure and the air density.

$$V = \sqrt{\frac{2 \cdot p_d}{\rho}} \quad (2.14)$$

V_0 is the reference velocity, which is calculated from the measured dynamic pressure at the entrance of the test section. The color scale is determined by the difference between the reference velocity V_0 and the cross section velocity V , divided by V_0 .

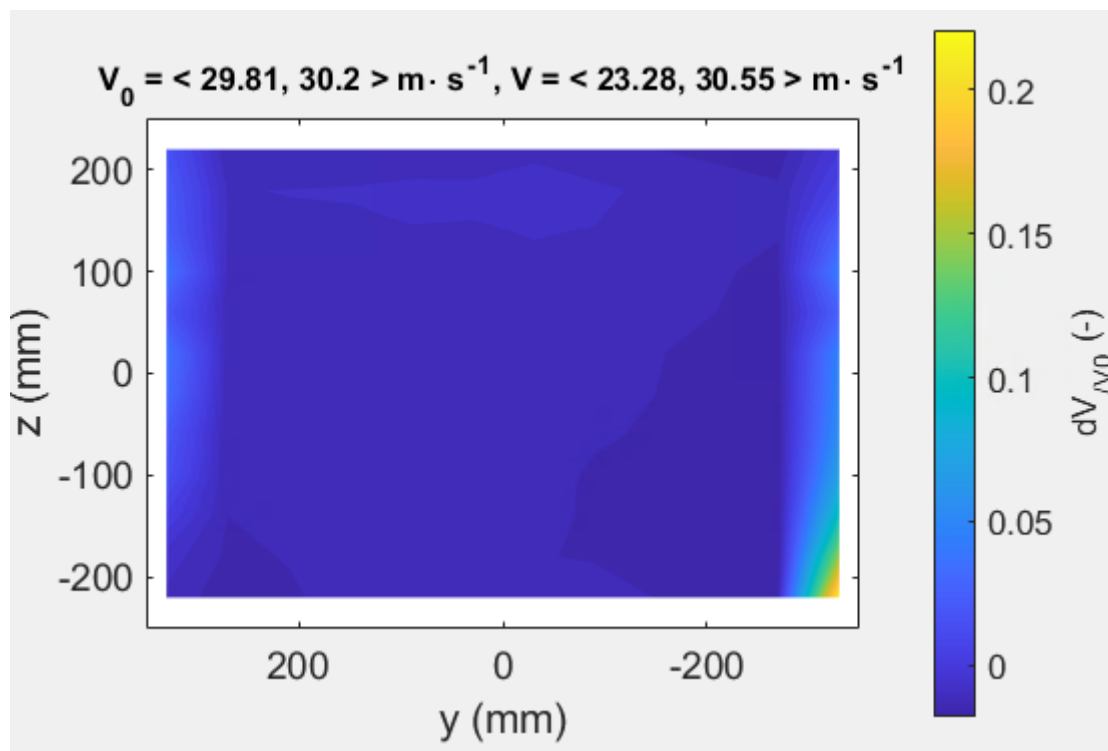


FIGURE 13: FLOW UNIFORMITY AT DISTANCE 755 MM INTO THE TEST SECTION

It stands out in Figure 13 that the only indications of boundary layers are on the left and right wall. While the grid was made as close to the walls as possible, it appears that for the top and bottom parts of the cross-section it was not close enough. Another note here is that the free flow velocity of the cross-section is compared with the reference velocity at the start of the test section, 755 mm in front of the cross section. Due to the boundary layer build up the average flow velocity further into the test section can be expected to be higher than at the start of it, which also follows from the negative values of dV/V_0 .

2.3.2 Dynamic pressure gradient

The airflow into the test section is determined by measuring the dynamic pressure at the start of the test section. While it is sometimes assumed that this dynamic pressure and consequently the flow velocity will be stable throughout the test section, in reality the flow stream size decreases due to a growing boundary layer on the test section walls, which increases the dynamic pressure and with that the flow velocity.

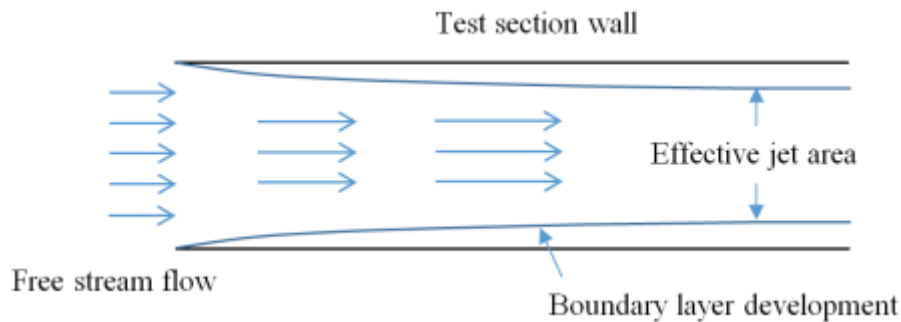


FIGURE 14: SCHEMATIC OF AIR FLOW IN A TUBE, EFFECT OF BOUNDARY LAYER



FIGURE 15: TEST SECTION, 5 GLASS WINDOWS [10]

Figure 15 shows the test section of the wind tunnel, with the 5 panels being the removable glass walls. One of the glasses contains a hole through which a Pitot probe was stuck to measure the dynamic pressure. This glass with the Pitot probe exchanged positions throughout the tests, to obtain dynamic pressure values for 5 different positions along the length of the test section. Each glass is 370 mm wide, with the tip of the Pitot tube approximately placed at the start of the second glass window, Figure 16 shows this more clearly.

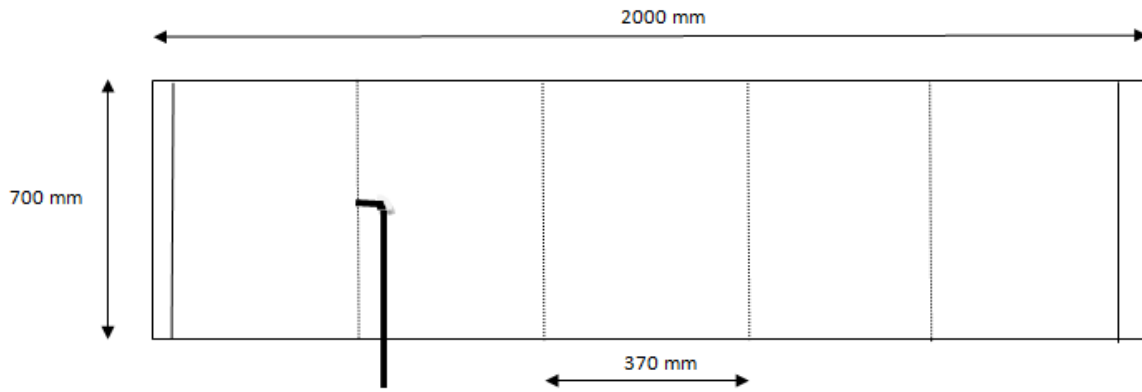


FIGURE 16: SCHEMATIC TOP VIEW OF THE TEST SECTION

At each position the indicated flow velocities from the conditioning chamber from 10 to 50m/s were measured, to then compare the dynamic pressure from the setting chamber to the dynamic pressure measured in the test section. The results of the calculated flow velocity for each section with initial velocities are displayed in Figure 17.

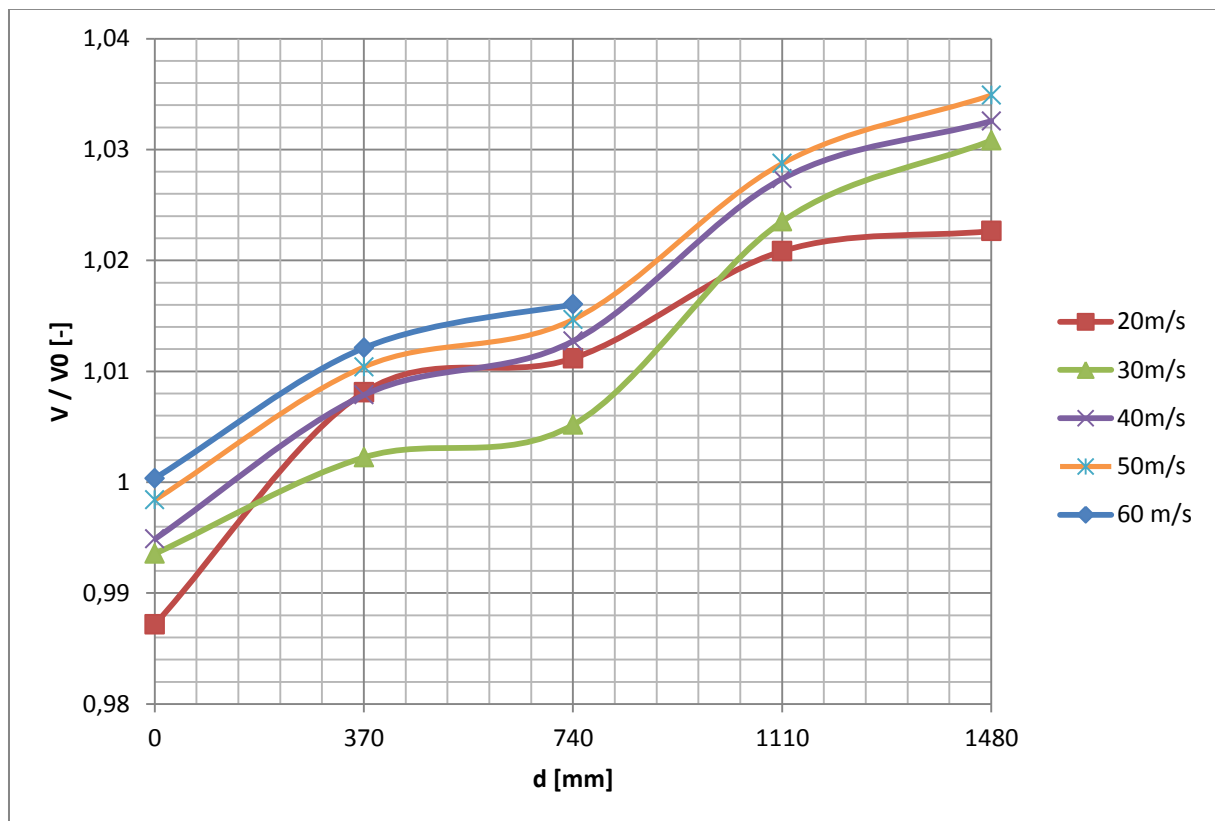


FIGURE 17: VELOCITIES PER LONGITUDINAL DISTANCE IN THE TEST SECTION. GROUPED PER INDICATED AIR SPEED

Through linear regression an equation could be set up to describe the expected velocity at a certain distance in the test section. This could be useful for future experiments, as it allows the

user to determine the free stream velocity around their model, instead of the free stream velocity at the start of the test section.

First, for each desired velocity a linear equation could be made, in the form of:

$$\frac{V(x)}{V_0} = c_1 x + c_2 \quad (2.15)$$

The intercept c_2 should in theory be equal to 1, as the speed at $x = 0$ should be equal to V_0 , the speed measured by the wind tunnel reference Pitot tube at the start of the test section. c_1 and c_2 are determined through linear regression, which then results in the following equation for the velocity at a certain distance x into the test section:

$$V(x) = 2.40136 \cdot 10^{-5} \cdot V_0 \cdot x + 0.996402 V_0 \quad (2.16)$$

Testing the equation above for correlation with the measured data yields a correlation coefficient of 0.999614, making R^2 0.999229, indicating a very good fit.

Relation turbine rotations and free flow velocity

The indicated V_0 term is rather not used for this wind tunnel, as the indicated value is derived partially with outside temperature values, and is therefore inaccurate. A better variable to use would be the rotations velocity of the turbine, as it is the only controllable part of the wind tunnel. From all measurements at different velocities a relation can be found between the turbine rotations and flow velocity at the start of the test section.

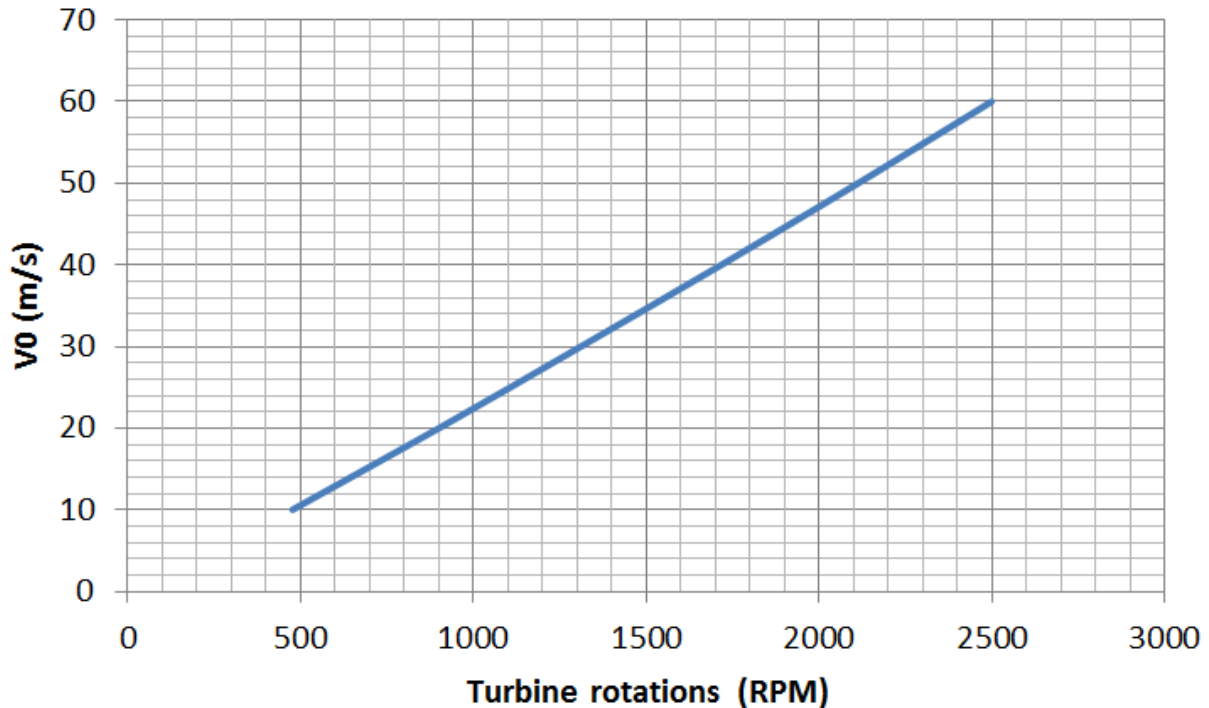


FIGURE 18: RELATION BETWEEN TURBINE ROTATIONS AND FREE FLOW VELOCITY

A linear fit would be sufficient for the range of 10 to 60 m/s, even though a polynomial fit would have been better for the full range. It was assumed that the very low velocities below 10 m/s are rarely used, and that the focus should be on having an as accurate as possible model for the higher ranges. The same equations to calculate the slope, intercept and errors are used as for the calibration constants of the pressure transducers.

$$s_{xx} = \sum_1^n (x_i - x_m)^2 = 2861264 \quad (2.17)$$

$$s_{yy} = \sum_1^n (y_i - y_m)^2 = 1750 \quad (2.18)$$

$$s_{xy} = \sum_1^n (x_i - x_m)(y_i - y_m) = 70752.7 \quad (2.19)$$

$$K = \frac{s_{xy}}{s_{xx}} = 0.02473 \frac{Pa}{mA} \quad (2.20)$$

$$B = y_m - Kx_m = -2.1833 Pa \quad (2.21)$$

The intercept reasonably should be at 0, as for 0 RPM there is no free flow velocity. However the relation between the RPM and V is not linear, it is merely approximated as a linear relation for the interval between 10 and 60 m/s.

$$\sigma_{yx}^2 = \frac{1}{n-2} \sum_1^n (y_i - y_{e i})^2 = 0.1111 \quad (2.22)$$

$$\sigma_K^2 = \frac{\sigma_{yx}^2}{s_{xx}} = 3.9 * 10^{-8} \quad (2.23)$$

$$\sigma_K = \text{Var}_K = 0.000197 \quad (2.24)$$

$$\sigma_b^2 = \sigma_{yx}^2 \left(\frac{1}{n} + \frac{x_m^2}{s_{xx}} \right) = 0.10631 \quad (2.25)$$

$$\sigma_b = \text{Var}_b = 0.32605 \quad (2.26)$$

$$\text{Regression}_{SS} = \sum_1^n (y_{e i} - y_m)^2 = 1748.67 \quad (2.27)$$

$$\text{Total}_{SS} = \sum_1^n (y_{o i} - y_m)^2 = \text{Regression}_{SS} + \sigma_{yx}^2 = 1749.55 \quad (2.28)$$

$$R^2 = \frac{\text{Regression}_{SS}}{\text{total}_{SS}} = 0.999746 \quad (2.29)$$

That makes the slope:

$$K = 0.02473 \pm 0.000197$$

$$B = -2.1833 \pm 0.32605$$

$$V_0 = 0.02473 \text{ RPM} - 2.1833 \quad (2.30)$$

Consequently, determining the rounds per minute required for a desired inlet velocity V_0 can be done with equation 2.31.

$$\text{RPM} = 40.4404 V_0 + 2.1833 \quad (2.31)$$

2.3.3 Flow angularity

While accelerating the air by means of the fan, the air will also be given an angular velocity due to the rotation of the fan blades. Also, as the wind tunnel in the institute is a closed loop version, the air will have to be guided in a loop. In the corners this is done by corner vanes, which assist the air to adjust its trajectory. This rotational movement of the air is undesired in the test section however, which is why a honeycomb grid right in front of the test section further decreases velocities in any other directions than the desired free stream flow along the length of the test section.

To measure the actual angular velocity of the free stream a 5-hole probe is used, for which a side view schematic is showing in Figure 19.

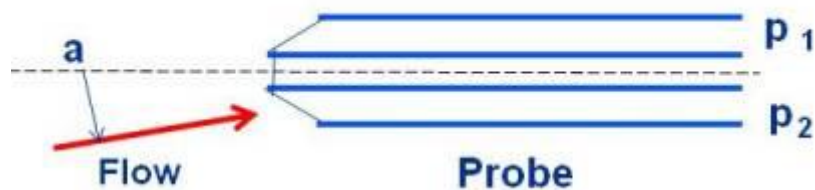


FIGURE 19: SCHEMATIC OF THE SIDEVIEW OF A FIVE HOLE PROBE [2]

The 5-hole probe consists of 5 tubes, one in the middle and 4 in a cross shape around it. The tubes around are cut off at a 45 degree angle to the middle tube, allowing air entry from a wider range. The flow coming towards the probe has an angle a , in case angle a is 0 all the tubes register the same pressure. However, if the flow enters at an angle the tubes will display a different pressure, from which the free flow angle can be determined.

$$p_1 - p_2 = f(a) \quad (2.32)$$

The exact function f is determined by calibrating the probe. Measurements of the angularity can be performed along the length of the test section, as well as in the cross sectional plane where the model will reside. During this thesis both the calibration of the 5-hole probe and flow angularity measurements were not performed due to the unusable state of the 5-hole probe.

2.3.4 Large scale fluctuations

For each test the dynamic pressure of the inlet flow into the test section is measured. For many experiments it is assumed that the inlet flow remains constant, and in general this should be the case.

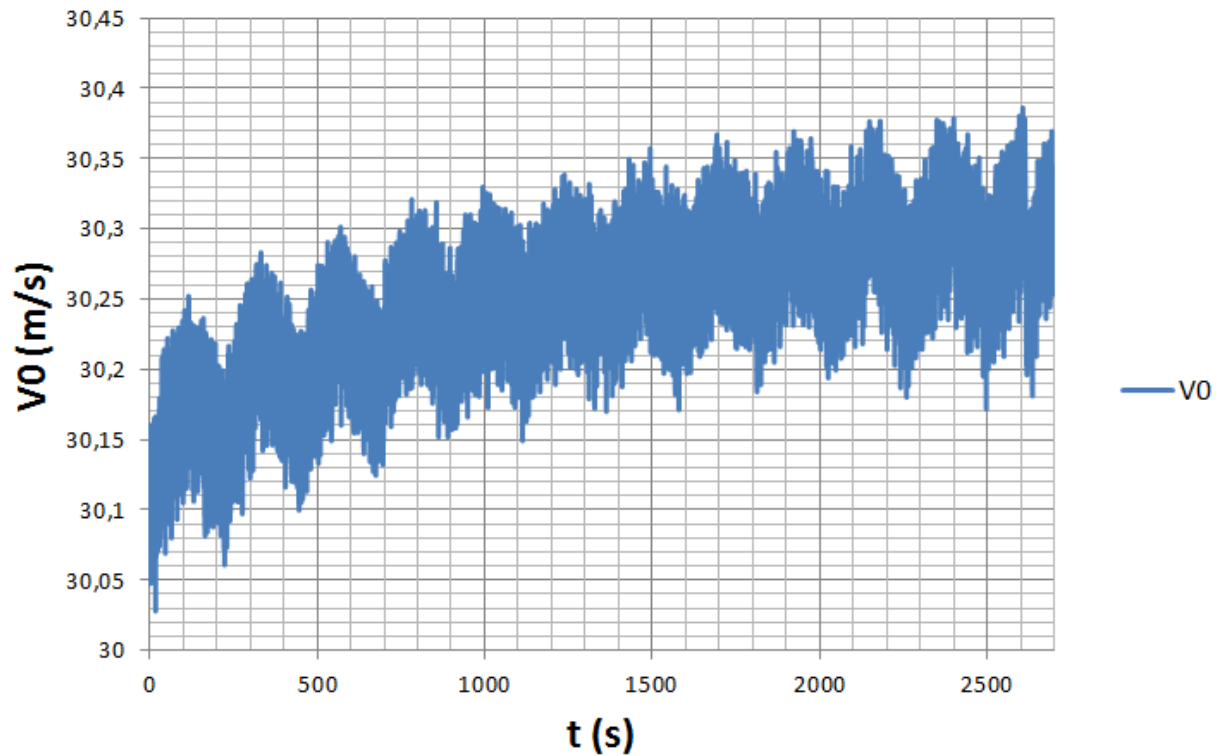


FIGURE 20: V0 OVER TIME, DESIRED VELOCITY OF 30 M/S, NO COOLING

In Figure 20 it can be seen that the inlet flow V_0 is not at all stable. There is a wave like change of the velocity with a period of 225 seconds, and a steady increase of the mean. For the sinusoid pressure change the measured dynamic pressure is investigated, shown in Figure 21.

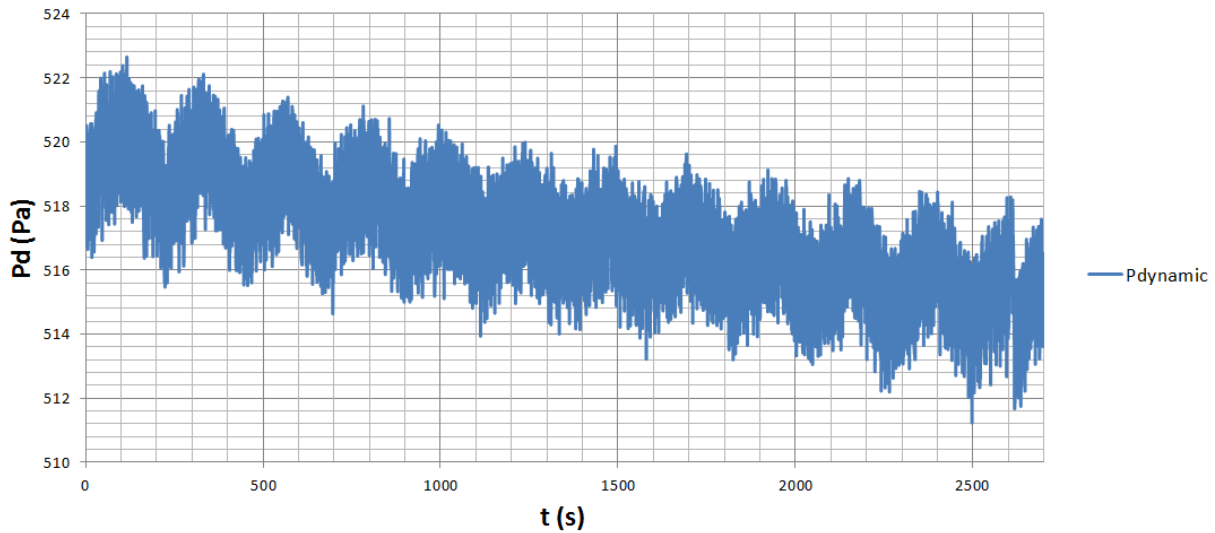


FIGURE 21: THE DYNAMIC PRESSURE OVER TIME AT THE ENTERANCE OF THE TEST SECTION. $V_0 = 30$ M/S, 1336 RPM.

The same sinusoid signal can be noticed, with the same periods. What stands out is the large difference between consecutive measurements, on average 1.79 Pa, making the uncertainty in a single measurement 1.09 Pa. In Figure 22 the fast four transform of the pressure signal is shown to possibly obtain more information on the frequency of vibrations. The most dominant frequency shown in the figure is the sinusoidal frequency that could be noticed from earlier figures.

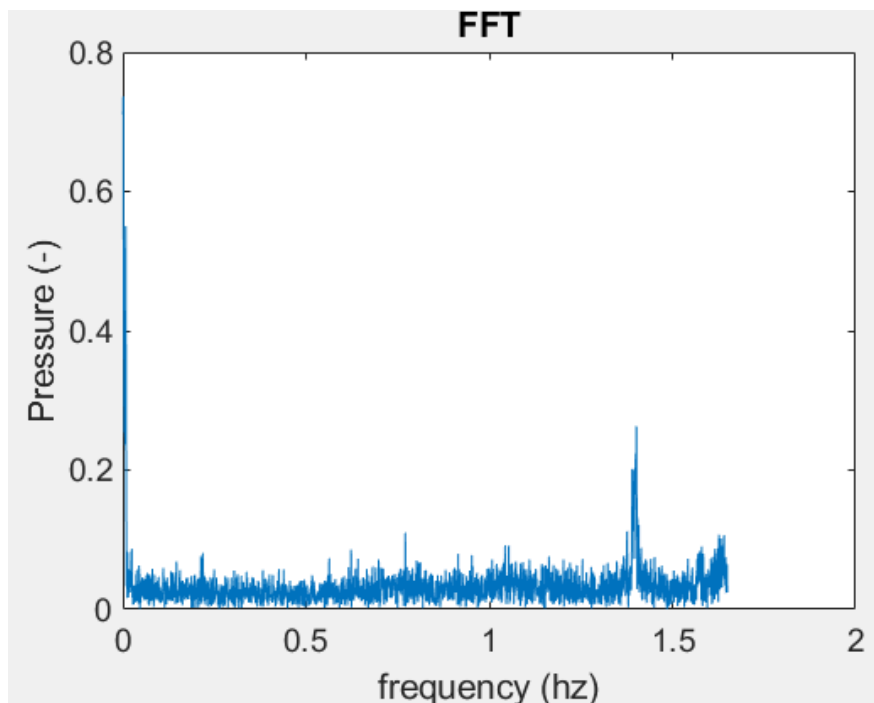


FIGURE 22: FAST FOURIER TRANSFORM OF THE REFERENCE DYNAMIC PRESSURE

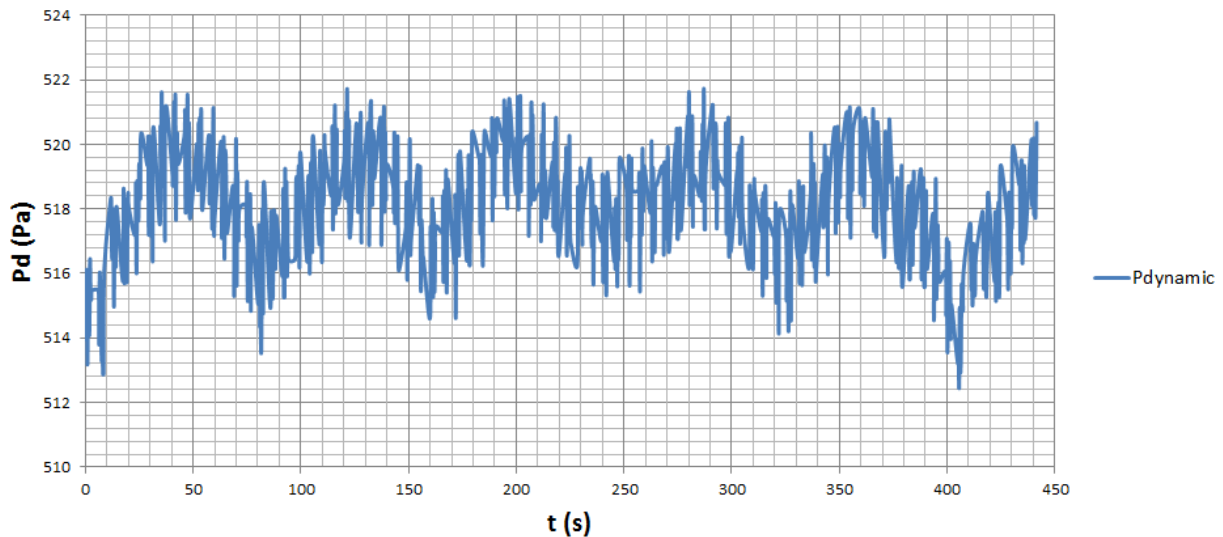


FIGURE 23: THE DYNAMIC PRESSURE OVER TIME AT TEST SECTION ENTERANCE. $V_0 = 30$ M/S, 1334.2 RPM

Figure 23 shows the dynamic pressure measurements of a similar but independent test, with the same desired inlet velocity of 30 m/s. A sinusoidal signal can again be recognized, though the period is much shorter, only 80 seconds. The amplitudes of the large waves are similar, for the first it is 3.25 Pa, for the second it is 3.75 Pa. This all suggests that the fluctuations are likely not caused by an inaccuracy in the wind tunnel structure, but rather by the PID controller trying to stabilize the velocity. It uses the V_0 that was chosen at the start of the test, and attempts to correct for any difference by changing the turbine rotations per minute, even though the system indicates that the rotations per minute are stable. The PID controller responsible for stabilizing the velocity appears to overshoot the target, and instead creates a marginally stable system. Likely the change of temperature over time is partially the cause of this.

Temperature

The temperature is measured by thermocouples in the flow conditioning and setting chamber. The temperature in the wind tunnel is supposed to be kept constant; however a rise over time can be expected unless the wind tunnel is actively being cooled. The interaction between the turbine and the air within the tunnel will steadily increase the air temperature, as well as the machines regulating the wind tunnel and devices around it will heat up the surroundings, which in turn affects the test section. The temperature is constantly measured by two thermocouples at the end of the conditioning chamber, as well as one on the outside of the wind tunnel (to measure the Lab temperature). The increase of temperature over time for a 45 minutes measurement can be seen in Figure 24.

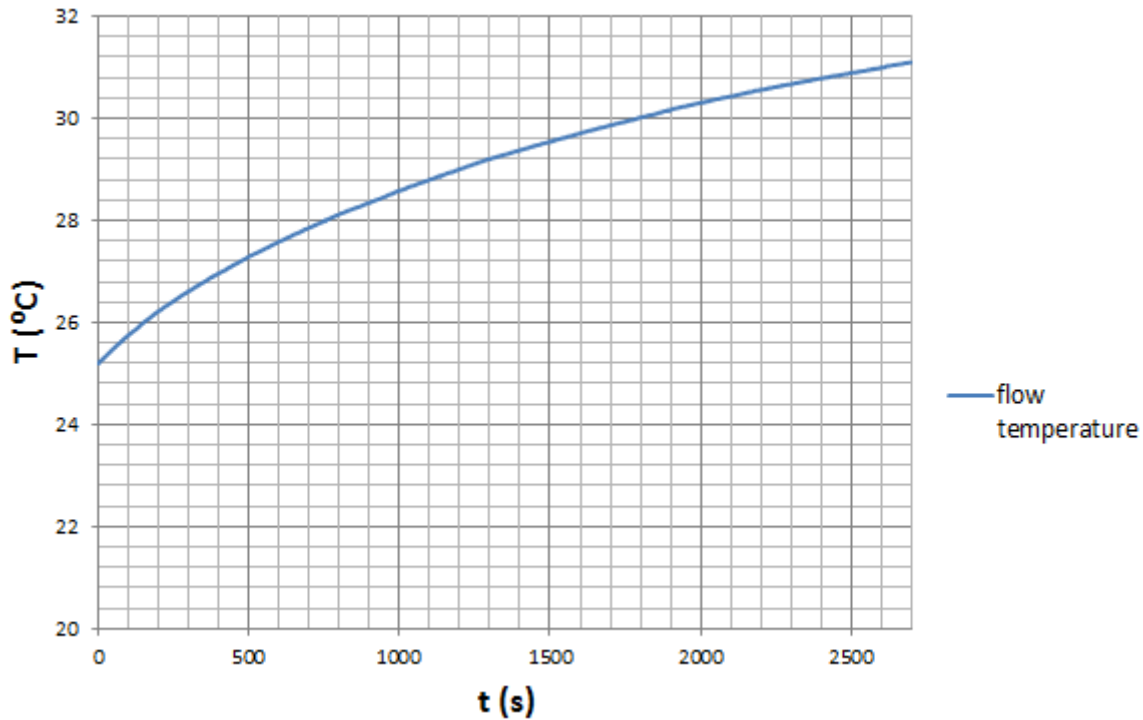


FIGURE 24: TEMPERATURE OVER TIME, 1336.2 RPM

During the 45 minute experiment the drive system was kept at a constant velocity of 1336.2 rounds per minute to generate an airflow velocity of 30 m/s at the test section entrance. The cooling system was not working; therefore a steady air temperature increase can be seen.

This directly affects the results however, as the temperature affects the pressure, air density and viscosity. The pressure difference is relatively minimal, as can be seen in Figure 25, however the air density change is not something that can be ignored, as it directly affects the dynamic pressure which is one of the main measurements performed in the wind tunnel.

$$\rho = \frac{P}{RT} \quad (2.33)$$

In equation 33 R is the air gas constant, 287.058 J/Kg K and the temperature T is expressed in Kelvin.

The wind tunnel computer system automatically calculates the density of the air within, but uses for that an average between the inner temperature and the ambient temperature. This density is then used to calculate the free flow velocity, which is then also inaccurate, and should only be used as a rough estimate. For the measurements in this thesis the density and velocities are determined only with the air temperature from within the wind tunnel.

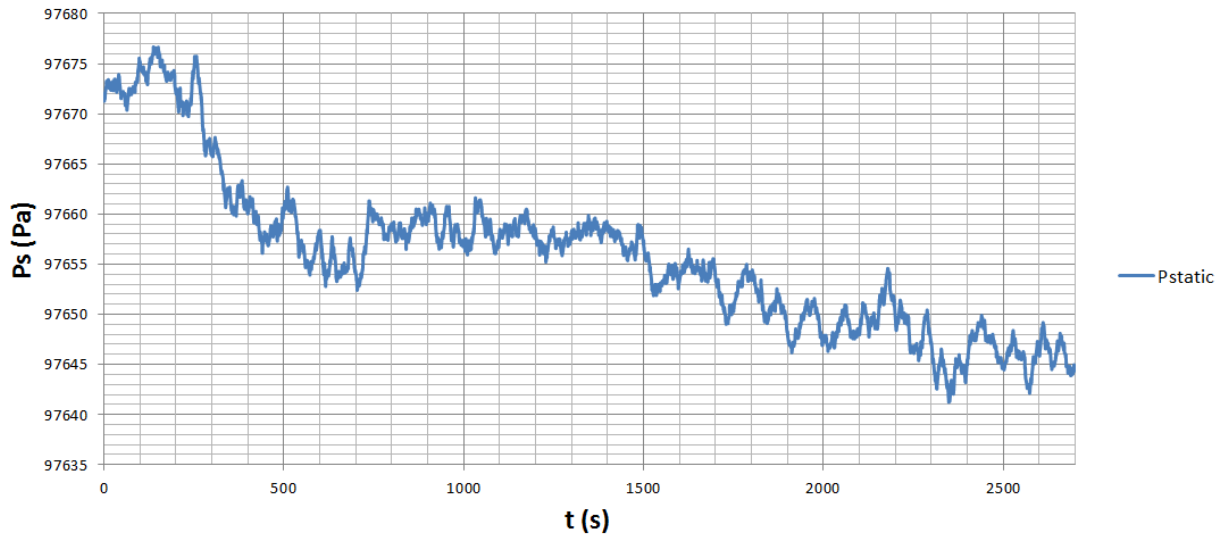


FIGURE 25: PRESSURE OVER TIME, 1336 RPM

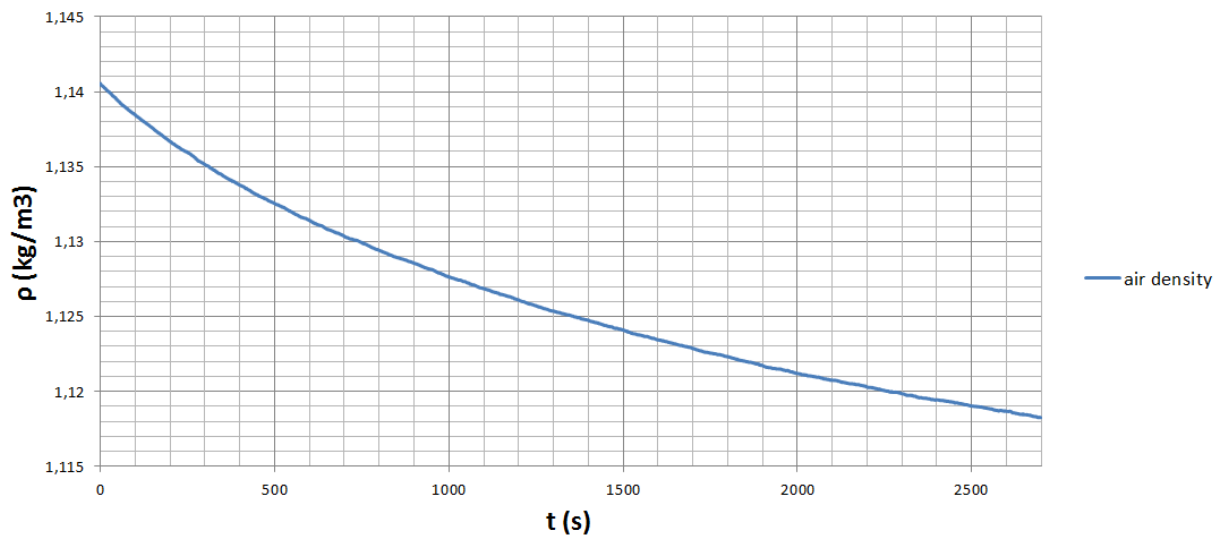


FIGURE 26: DENSITY OVER TIME, 1336 RPM

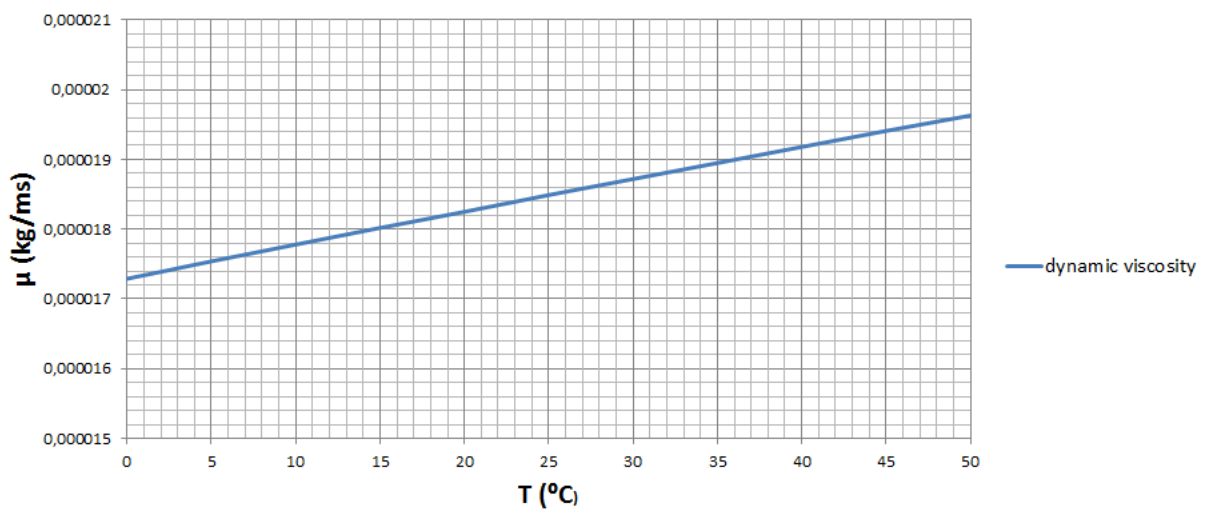


FIGURE 27: DYNAMIC VISCOSITY OVER TIME, 1336 RPM

For the consistency of results the cooling should be working during long measurements, as without it the temperature difference over time will affect the results.

3 Calibration report

The main goals of a calibration report are to help a future user of a device or machine to quickly and easily find accurate information about the working state of said device or machine. In case of the wind tunnel set-up at the Institute of Aerospace Engineering it is important that the report contains information about the measurement devices used in the wind tunnel, as well as any information about the airflow through the test section.

The first page should contain as much information as possible for a quick look, without becoming unwieldy. It shows clearly which equipment the report is made for, who is the main responsible person for the report and the date of publication. Further down the page the table of contents is located. It contains the most basic information about the measurement devices and section calibrations, such as their name, primary function, calibration date and page number where the calibration results can be found together with additional information.

For each of the instruments the following points are highlighted:

- Model and serial number of the instrument
- Tag code (if applicable)
- Work area
- Name of the responsible technician
- Date of the calibration
- Ambient conditions at the moment of calibration
- Model and serial number of the calibration device used
- Range of the instrument
- Calibration constants with errors

For the section calibration the following are highlighted:

- Name of section calibration
- Date of calibration
- Ambient conditions at the moment of calibration
- Relevant instruments used for calibration (and their specific function)
- Short description of calibration technique

Calibration frequency for now should be based on a set time, which is why the date of the calibration is specifically mentioned. Future users are easily able to see when the last calibration was performed, and should be able to know whether the instruments are user ready or need to be recalibrated. A usage based calibration would probably be better, but usage of the wind tunnel is hard to keep track of, so this would be difficult to implement.

The full calibration report can be seen in Appendix A.

4 Test measurement

A simple measurement of a model car is conducted to investigate the usefulness of the calibrations. The forces on the car will be measured by the load sensor mounted to the car while at the same time the wake of the car is measured by a movable Pitot tube.



FIGURE 28: CAR MODEL SET-UP

4.1 Model

The investigated model is a scaled down version of the Skoda Superb, a Station wagon of Czech design. The original car is scaled down by factor 10 to fit in the wind tunnel test section. The test section walls are limiters, but also the blockage ratio of the model inside the section. Whereas in the outside situation air around the car has infinite space, in the tunnel there are the wall sections that limit the air flowing around the car. Scientists in general stick to a maximum blockage ratio, the ratio of model cross-sectional area divided by the test section cross-section area, of between 5% and 10%[4]. The scale of 1:10 of the real Skoda Scala results in the following dimensions for the model:

TABLE 4: MODEL DIMENSIONS

	Length (mm)	Height (mm)	Width (mm)
model	481	137	182

The total cross-sectional area is given by the height multiplied with the width;

$$A = H * W = 137 * 182 = 24934 \text{ mm}^2 \quad (4.1)$$

For the test section cross-section this is:

$$500 * 700 = 350000 \text{ mm}^2 \quad (4.2)$$

$$\text{Blockage ratio} = \frac{A_{car}}{A_{section}} = \frac{24934}{350000} \quad (4.3)$$

$$\text{Blockage ratio} = 0.0712 = 7.12\% \quad (4.4)$$

4.2 Force measurement device

The sensor used, an Ati mini 40-a is able to recognize forces in 6 degrees of freedom, for all possible translations and rotations. The positive X axis of the sensor is pointing to the front of the car, which then makes the negative x forces measured the drag force. The positive y axis is to the left of the car, which consequently makes the positive Torque moment around the Y axis show downwards rotation for the car's front wheels. The positive Z axis is upwards from the car, measuring lift. The negative values are consequently down force. In general throughout this project Fx and Fz will not be renamed, in case drag force or down force are used then respectively $-F_x$ and $-F_z$ are meant.

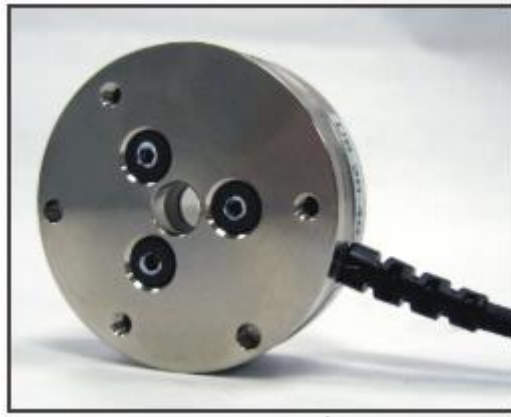


FIGURE 29: ATI MINI 40-A

Table 5 shows the ranges and errors of the sensor.

TABLE 5: SENSING RANGE OPTIONS FOR THE SENSOR

Calibration	F _x (N)	F _y (N)	F _z (N)	T _x (Nm)	T _y (Nm)	T _z (Nm)	F _x (N)	F _y (N)	F _z (N)	T _x (Nm)	T _y (Nm)	T _z (Nm)
Si-20-1	20	20	60	1	1	1	0.25	0.2	0.45	0.0125	0.0125	0.02
Si-40-1	40	40	120	2	2	2	0.5	0.4	0.9	0.025	0.025	0.04
Si-80-1	80	80	240	4	4	4	1	0.8	1.8	0.05	0.05	0.08
Sensing ranges							Error					

In Table 5 three calibration options are given, with accompanying sensing ranges and errors. For all the measurements in this project the most course calibration, Si-80-1, has been used due to the higher limit, especially with respect to the moment T_y.

The sensor is sensitive, so a plate is mounted on top of it which will be fastened to the car. This intermediary solution is chosen to decrease the handling of the sensor, which reduces the chances of damage. The plate was created in Solidworks and after that printed with a Prusa 3d printer. The plastic is less stiff than a metal version would be, but the influence was deemed too insignificant to actually make a metal plate.

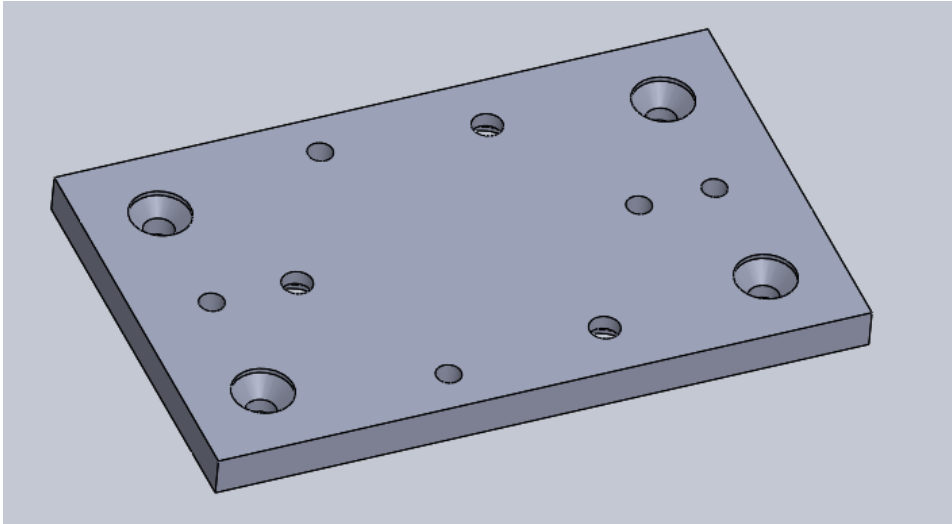


FIGURE 30: MODEL OF PLATE

Three threaded holes in the middle circle connect the plate to the sensor. The four holes in the corner are for screws that connect the sensor and plate to the car model. These screws can be reached without touching the sensor.



FIGURE 31: MODEL CAR FROM THE BOTTOM

Figure 31 shows the bottom of the model, with in the middle a hole where the sensor and plate are placed. The total setup looks as follows:

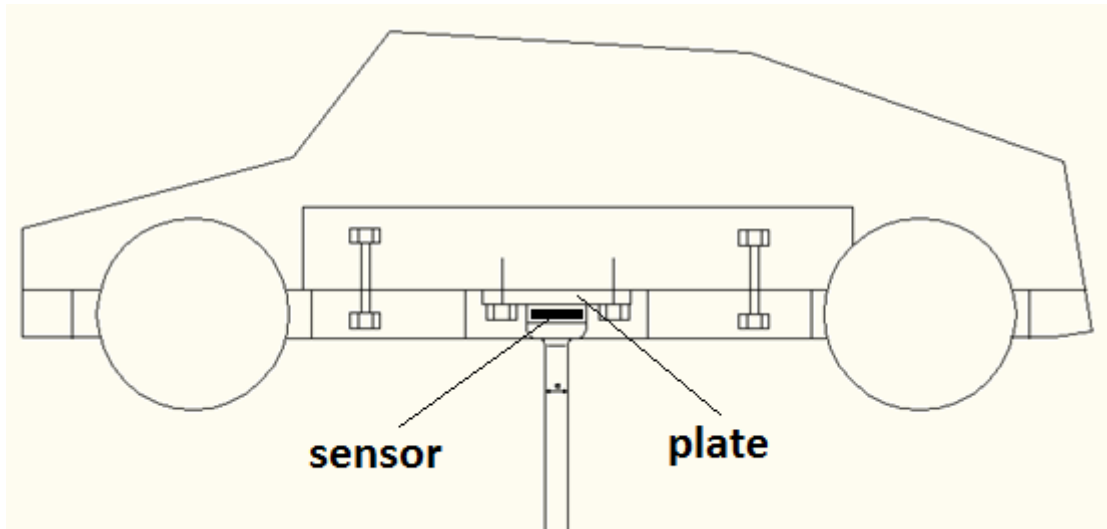


FIGURE 32: SCHEMATIC OF THE MODEL, SENSOR AND MOUNTING

The model is mounted from the direction of the Z axis. This allows for rotation around that same axis, which can be used during measurements to investigate the influence of the yaw angle of the model on the forces and moments. The choice was made to have a mount from the bottom, to have as little interference on the flow around the car as possible.

The model is placed a few millimeters above the bottom panel of the test section. This does pose some differences to the real world situation, primarily to the boundary layers. In the real situation the car can be considered standing still while everything around it (air, road) moves with the driving speed in v_∞ direction (Figure 33, situation A). For the model however the car is actually standing still, but so is the road. The boundary layer can be seen in Figure 33, situation B.

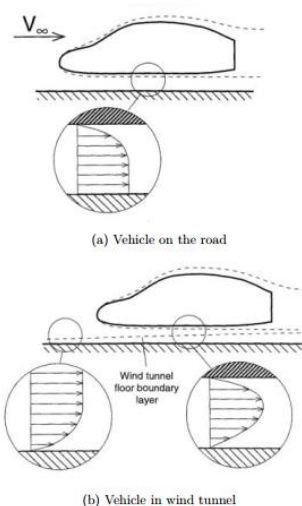


FIGURE 33: BOUNDARY LAYER SITUATIONS

4.3 Load and wake measurements

The load and wake measurements are performed at the same time so that the results can be compared. The forces on the car are measured using the ATI mini 40-a load sensor, while the wake is measured in a grid 150 mm behind the model by a movable Pitot tube. The measurements on the model were performed at a free speed velocity of 30 m/s. At first a coarse grid is used, for which measurements are made 50 mm apart from each other, up to 250 mm from the middle, and 300 mm high from the bottom glass wall. The model car only reaches 90 mm from the middle on both sides. The lowest measurements, made as close as possible to the bottom glass wall, are clearly affected by the boundary layer.

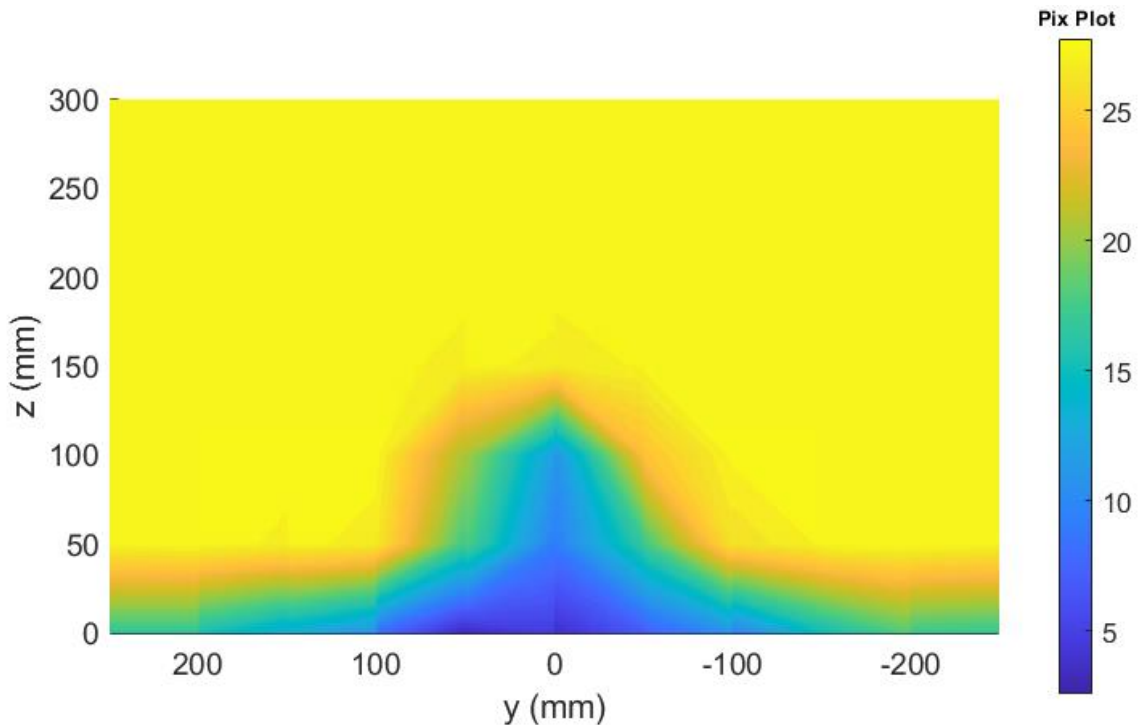


FIGURE 34: COURSE GRID OF WAKE VELOCITY

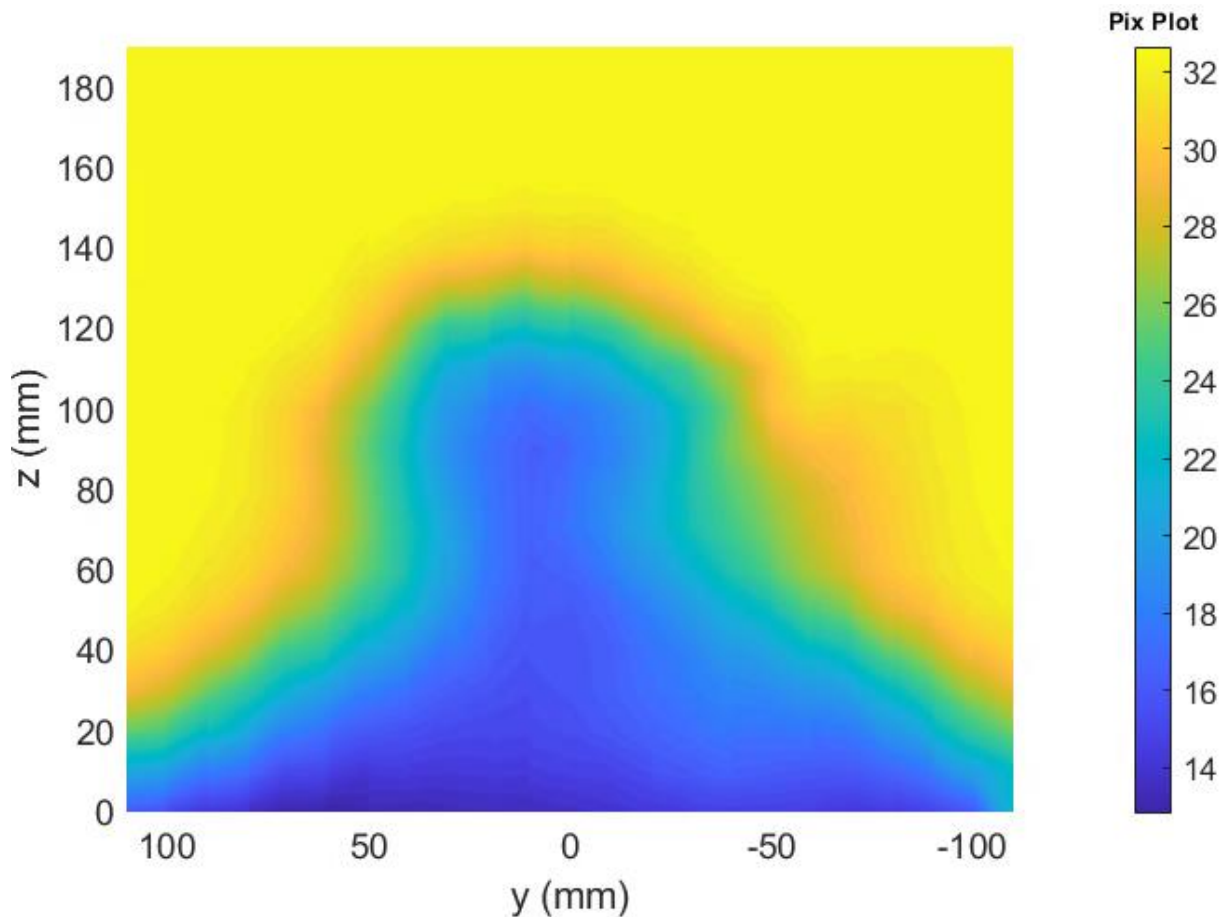


FIGURE 35: FINE GRID

The grid used to obtain Figure 35 consists of measurement points 10 mm apart. At each point 10 measurements are made, 0.3 seconds after each other, which are in the end averaged to reduce the error. For each of these the temperature in the conditioning chamber, static pressure in the conditioning chamber, dynamic pressure at the start of the test section and the dynamic pressure at the current point on the grid are measured and saved. The drag force $-F_x$ can then be calculated through the total velocity loss in the wake behind the car.

$$F_D = \iint \rho V da (V_0 - V) \quad (4.5)$$

$$F_D = \iint (\rho V V_0 da - \rho V^2 da) \quad (4.6)$$

$$F_D = \frac{1}{2} \rho c_d A V_0^2 \quad (4.7)$$

$$c_{D0} = 2 \iint \frac{V}{V_0} \frac{dA}{S} - \frac{V^2}{V_0^2} \frac{dA}{S} \quad (4.8)$$

In general with V_0 the entry velocity into the test section is meant. However in the chapter of dynamic pressure distribution it is shown that the free flow velocity increases over the length of test section as a result of growing boundary layers. An equation was found to predict the velocity at a point x along the length of the test section based on the inlet velocity V_0 . By using V_x instead, with x being 755 mm, a more accurate of the effect the car has on the air flow behind it, from which the drag coefficient is determined.

$$V(x) = 2.40136 \cdot 10^{-5} \cdot V_0 \cdot x + 0.996402 V_0 \quad (4.9)$$

$$P_D = \frac{1}{2} \rho V^2 \quad (4.10)$$

$$V = \sqrt{\frac{2P_D}{\rho}} \quad (4.11)$$

$$c_{D0} = 2 \iint \left(\sqrt{\frac{P_D}{P_{D0}}} - \frac{P_D}{P_{D0}} \right) \frac{dA}{S} \quad (4.12)$$

This brings profile drag coefficient measured by the wake to $c_{D0} = 0.2371$.

The drag coefficient can be compared to the one derived from the load sensor that was operating at the same time. The sensor measured forces in 3 directions, as well as 3 torques around those axis. It conducted measurements 500 times per second, over a span of 14 seconds. As the wind conditions are somewhat constant over that time it was possible to average out the measurement results gained over the 14 second span, which can be seen in Table 6

TABLE 6: AVERAGE FORCES AND MOMENT FOR V 30 M/S

	Fx (N)	Fy (N)	Fz (N)	Tx (Nm)	Ty (Nm)	Tz (Nm)
mean	-4,87454	-0,36474	-1,15021	0,011999	0,408461	0,009607
variance	0,162578	0,117789	0,311238	0,000545	0,010587	0,002309

From the loads the force and moment coefficients can be derived, through equations 4.13 to 4.15.

$$F = \frac{1}{2} \rho * A * c * V^2 \quad (4.13)$$

$$M = \frac{1}{2} \rho * A * c * V^2 * L \quad (4.14)$$

$$c = \frac{2 * F}{\rho * A * v^2} \quad (4.15)$$

TABLE 7: COEFFICIENTS FOR THE DIFFERENT FORCES AND MOMENTS

	F _x	F _y	F _z	T _x	T _y	T _z
c	-0,38093	-0,0285	-0,08989	0,001949	0,066362	0,001561
±	0,012705	0,009205	0,024323	8,86E-05	0,00172	0,000375

From Table 7 it follows that the drag coefficient c_D measured by the load sensor is 0.381, which is significantly different from the drag coefficient measured through the wake method. Skoda itself claims a 0.27 profile drag coefficient value for the Skoda Superb [14].

5 Evaluation

The profile drag coefficient found through the wake measurements ended up being 0.2371. This is after taking the lessons learned during calibration into account, like the increasing velocities along the length of the test section, or the increasing temperature over time. As mentioned in the chapter 2.3.4 Large scale fluctuations the wind tunnel computer uses an average of the outside temperature and tunnel temperature to determine the air density, which is then used to calculate the flow velocities.

TABLE 8: VALUES OF C_{D0} DEPENDING ON THE PERFORMED CALIBRATION

	Old	P, T adjusted	TRUE
Cd0	0,2697	0,2018	0,2371
% difference from true	13,7	-14,9	0,0

Table 8 shows the values of obtained profile drag coefficients from the wake measurements depending on which calibrations were performed and applied in the calculations. The first result is with the old calibration constants from before the recalibration, and without adjusting for the temperature or velocity increase over the distance of the test section.

The second result is with the new calibration constants used for the pressure transducers, as well as with our own calculated density and velocities instead of using what the computer displays.

The last value is calculated with all the changes applied. Comparing this to the drag coefficient given by Skoda of 0.27 [14] still sees a significant difference. This can partially be attributed to the imperfect set up in the wind tunnel, as the model was placed on a pole, a few millimeters above a non-moving glass wall with still wheels. This is not comparable to real life conditions [8] where there is a moving asphalt ground with moving wheels, no extra parts and a different Reynolds number due to size difference.

The reason for the large difference between the drag coefficients calculated by the force sensor method compared to the wake method was not found. Both methods were executed at the same time, and thus had the same conditions. In theory the wake method should have yielded the higher drag coefficient, as it falsely attributed the boundary layer effect as a result of the wake of the car, while the boundary layer on top of the glass wall would have been there as well without the car model. More time and experiments will be needed to find the answer to this.

6 Conclusion

In this thesis the topic of calibration of devices and sections has been investigated in relation to the wind tunnel at the Brno Institute of Aerospace Engineering. The pressure transducers used for the measurements have been tested and recalibrated. Calibration sheets were made to present the results as clearly and concisely as possible. Using the newly calibrated instruments the test section of the wind tunnel was calibrated, which included measurements to describe dynamic pressure gradient, uniformity of flow in a cross-sectional area and large scale fluctuations. A calibration report template was proposed to simplify the process of checking for detailed information about the wind tunnel and the state of its instruments for future users. The report is missing the chapters on calibration of the flow angularity, which was not performed due to faulty equipment. This chapter will need to be added in the future to have the complete information about the air stream in the wind tunnel test section.

For the last chapter the information gained from the calibrations was applied in a typical wind tunnel test to investigate the influence of the changes. Both the instrument calibrations and the section calibrations resulted in an over 10% difference in the final value, which supports the usefulness of these calibrations.

Bibliography

- [1] BARLOW, J.B., RAE, W.H. and POPE, A., 1999. *Low-Speed Wind Tunnel Testing*. 3rd ed. Wiley & Sons ISBN 0-471-55774-9.
- [2] BLOCKLEY, R. and SHYY, W., 210. *Encyclopedia of Aerospace Engineering*. Wiley ISBN 978-0-470-75440-5.
- [3] CATTAFESTA, Louis, BAHR, Chris and MATHEW, Jose, 2010, Fundamentals of Wind-Tunnel Design. *Encyclopedia of Aerospace Engineering* [online]. 15 December
- [4] GE Sensing and Inspection Technologies., 2008. *Druck DPI 610/615 IS User Manual*. 2nd ed.
- [5] GLEGG, S. and DEVENPORT, W., 2017. *Aeroacoustics of Low Mach Number Flows: Fundamentals, Analysis and Measurement*. Academic Press ISBN 9780128096512.
- [6] HALL, N., 2021. *Five Hole Probe - Flow Direction*. National Aeronautics and Space Administration. May 13 2021, Available from: <https://www.grc.nasa.gov/www/k-12/airplane/tunp5h.html>.
- [7] HUCHO, W., 19877. *Aerodynamics of Road Vehicles. from Fluid Mechanics to Vehicle Engineering*. 1st ed. Butterworth-Heinemann Ltd ISBN 0-408-01422-9.
- [8] KATZ, J., 2016. *Automotive Aerodynamics*. Wiley ISBN 9781119185734.
- [9] KATZ, J., 1994. *Race Car Aerodynamics : Designing for Speed*. US: Bentley Inc. ISBN 9780837601427.
- [10] LAJZA, O., 2014. *Aircraft Engine Cooling System Testing*. Master ed. Brno University of Technology.
- [11] LYU, Z., 2018. *Aerodynamic Wind Tunnel in Passenger Car Application*.
- [12] MONTGOMERY, D.C. and RUNGER, G.C., 2011. *Applied Statistics and Probability for Engineers*. 5th edition ed. New York: Wiley ISBN 978-1118539712.
- [13] POPE, A., 1961. *AGARDograph 54: Wind Tunnel Calibration Techniques*. NATO: , April 1961.
- [14] škoda, 2020. *Skoda Storyboard - Skoda Superb*. 26.10.2020, Available from: <https://www.skoda-storyboard.com/en/skoda-model/superb/>.
- [15] TIFFORD, A.N., 2012. Wind-Tunnel Cooling. *Journal of Aeronautical Sciences*, vol. 10, no. 3, pp. 98.
- [16] TOULOUKIAN, Y.S. and P.E. LILEY, S.C.S., 1970. *Thermophysical Properties of Matter and Substances v 3, Thermal Conductivity; Nonmetallic Liquids and Gases*. New York: IFI/Plenum.

Nomenclature

P	pressure
K	multiplicative calibration constant
B	additive calibration constant
x_i	measured x
x_m	mean x
s_{xx}	sum of square error for x
s_{yy}	sum of square error for y
s_{xy}	sum of square error for x and y combined
σ_{yx}	residual sum of squares
R	correlation coefficient
σ	standard deviation
ρ	density of air
R	air gas constant
T	temperature
V	air velocity
p_D	dynamic pressure
V_x	air velocity at distance x into the test section
V_0	air velocity at entrance of the test section
RPM	turbine rotations per minute
t	time
A	(cross-sectional) area
H	Height
W	width
F_i	Force in i direction
T_i	Torque around i axis
F_D	Drag force
C_D	Drag coefficient
C_{D0}	Profile drag coefficient
P_{D0}	Dynamic pressure at entrance

Appendix A

Calibration Report			
General			
Tag:		Module:	Free flow characteristics
Area:	Wind tunnel IAE	Report Number:	1
Technician:	Hendrik de Boer	Date of Calibration:	14-5-2021
Work Order:	CAL	Printed:	
Measurement devices			
Utility	Name	Date	Page
Pressure	PX665 - 10D1	17-5-2021	2
	PX665 - 50D1	17-5-2021	4
	PX665 - 25 BD1	17-5-2021	6
	PX665 - 01D1	17-5-2021	8
Temperature			
Force	ATIMini 40-A		
Section calibration			
Utility		Date	Page
Longitudinal velocity distribution		18-5-2021	
Crosssectional uniformity		16-5-2021	
Flow angularity			
Turbulence			
Large scale fluctuations		16-5-2021	
Comments			
Date:		Approved by:	

PX 655 10D1				
General				
Tag:		Support module:		
Area:	VUT windtunnel	Routine:		
Hookup:		Report Number:	1	
Loop Diagram:		Date of Calibration:	14-5-2021	
Technician:	Hendrik de Boer	Printed:		
Work Order:		Ambient Temp:		
Cal model Num:	Druck DPI 650	Cal Serial Num:		
Instrument				
model:	PX 655 10D1	Error calculation		
serial number:	X15120190	Pass/Fail tolerance	0,5	
input:	0-2490 Pa	Out put:	4-20 mA	
Calibration Data				
Cal points	Output mA	Input mA	Error %	Status
2343			9,358	
2100			7,817	
2000			7,177	
1900			6,541	
1800			5,915	
1697			5,238	
1590			4,549	
1480			3,833	
1387			3,237	
1300			2,569	
1203			2,041	
1100			1,369	
1004			0,763	
884			-0,015	
805			-0,525	
692			-1,234	
596			-1,862	
500			-2,488	
401			-3,119	
300			-3,779	
204			-4,392	
102			-5,066	
1			-5,721	
Comments				
druck total ambient pressure			97362 t	25,9
machine			97392	
K =1 b =0				
Date:		Approved by:		

PX 655 10D1

Constants

K:	155,1890	B:	886,5650
K error:	0,1820	B error:	0,8310
Correlation	0,999985	R ²	0,999971

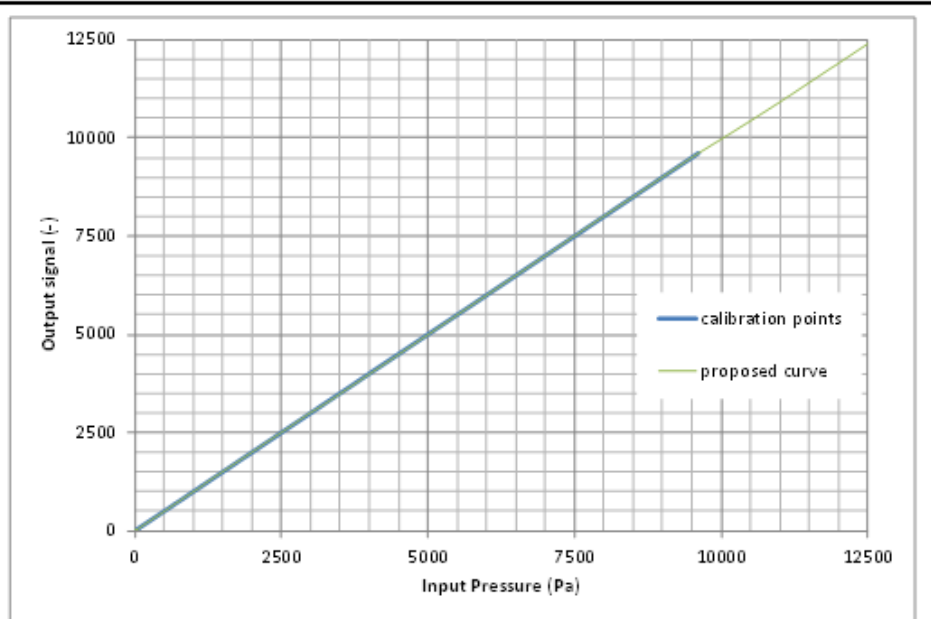
PX 655 50D1					
General					
Tag:		Support module:			
Area:	VUT windtunnel	Routine:			
Hookup:		Report Number:	2		
Loop Diagram:		Date of Calibration:			
Technician:	Hendrik de Boer	Printed:			
Work Order:		Ambient Temp:			
Cal model Num:	Druck DPI 650	Cal Serial Num:			
Instrument					
model:	PX 655 50D1	Error calculation			
serial number:	X12300013	Pass/Fail tolerance	0,5		
input:	0-12500 Pa	Output:	4-20 mA		
Calibration Data					
Cal points	Output Pa	Input Pa	Error %	Status	
1160		1160	1141,122	1,627413793	Fail
730		730	712,071	2,456027397	Fail
555		555	533,669	3,843423423	Fail
450		450	425,117	5,529555556	Fail
340		340	317,149	6,720882353	Fail
200		200	179,733	10,1335	Fail
102		102	77,1	24,41176471	Fail
50		50	23,404	53,192	Fail
0		0	0,006		
3360		3360	3347,486	0,372440476	Passed
2976		2976	2984,262	0,277620968	Passed
2703		2703	2701,459	0,057010729	Passed
2350		2350	2346,718	0,139659574	Passed
2020		2020	2015,003	0,247376238	Passed
1580		1580	1573,913	0,385253165	Passed
1196		1196	1186,312	0,810033445	Fail
9614		9614	9645,757	0,003303204	Passed
9130		9130	9167,068	0,004060022	Passed
8520		8520	8549,711	0,003487207	Passed
7949		7949	7981,54	0,004093597	Passed
Comments					
K= 777.44 B= -3098. previous results from Jiri, calibrations 2016					
Date:			Approved by:		

PX 655 50D1

Constants

K:	772,7707	B:	-3059,4820
K error:	0,4019	B error:	3,4476
Correlation	0,999998	R ²	0,999995

Proposed curve



Comments

Date: 14-5-2021 Approved by:

PX 655 25BDI				
General				
Tag:		Support module:		
Area:	VUT windtunnel	Routine:		
Hookup:		Report Number:	3	
Loop Diagram:		Date of Calibration:	14-5-2021	
Technician:	Hendrik de Boer	Printed:		
Work Order:		Ambient Temp:		
Cal model Num:	Druck DPI 650	Cal Serial Num:		
Instrument				
model:	PX 655 25BDI	Error calculation		
serial number:	X12160090	Pass/Fail tolerance	0,5	
input:	0-6230 Pa	Output:	4-20 mA	
Calibration Data				
Cal points	Output mA	Input mA	Error %	Status
-1			-6196,22	
142			-6196,03	
260			-6195,88	
362			-6195,74	
420			-6195,67	
520			-6195,53	
628			-6195,39	
716			-6195,28	
816			-6195,15	
955			-6194,97	
1077			-6194,82	
1211			-6194,64	
1328			-6194,49	
1484			-6194,29	
1690			-6194,02	
1904			-6193,74	
2237			-6193,32	
2707			-6192,71	
3323			-6191,92	
4005			-6191,05	
4745			-6190,09	
5370			-6189,28	
Comments				
K =1 b =0				
Date:		Approved by:		

PX 655 25BDI

Constants

K:	775,2690	B:	4803727,0000
K error:	0,5280	B error:	3272,7550
Correlation	0,999995	R ²	0,999991

PX 655 01D1				
General				
Tag:		Support module:		
Area:	VUT windtunnel	Routine:		
Hookup:		Report Number:	4	
Loop Diagram:		Date of Calibration:	14-5-2021	
Technician:	Hendrik de Boer	Printed:		
Work Order:		Ambient Temp:		
Cal model Num:	Druck DPI 650	Cal Serial Num:		
Instrument				
model:	PX 655 01D1	Error calculation		
serial number:	X15330124	Pass/Fail tolerance	0,5	
input:	0-249 Pa	Out put:	4-20 mA	
Calibration Data				
Cal points	Output mA	Input mA	Error %	Status
1			-5,553	
20			-4,235	
42			-2,86	
64			-1,444	
86			0,025	
102			1,124	
125			2,49	
148			3,758	
177			5,775	
205			7,58	
221			8,675	
Comments				
Date:		Approved by:		

PX 655 01D1			
Constants			
K:	155,1890	B:	86,5280
K error:	0,0880	B error:	0,4170
Correlation	0,999857	R ²	0,999714



Detailed Certificate of Calibration

Equipment Calibrated	NIST Traceability Information
Description: Six-Axis Force/Torque Sensor	NVLAP Lab Code: 200495-0
Manufacturer: ATI Industrial Automation	Cal Standard: REF – 1000
Serial Number: FT32856	Cal Standard: REF – 1001
Model: Mini40	Cal Standard: REF – 1183
Calibration: SI-80-4	Cal Standard: REF – 1119
Electronics: Net F/T	
Gain Multiplier: 100%	

Equipment Condition and Notes: Factory new.

Calibration Results: Passed
 Offset: Normal
 Gain: Normal

Calibrated Ranges (±):

Fx	Fy	Fz	Tx	Ty	Tz
80 N	80 N	240 N	4 N-m	4 N-m	4 N-m

Measurement Uncertainty (95% confidence level, percent of full-scale load):

Fx	Fy	Fz	Tx	Ty	Tz
1.50%	1.25%	1.50%	1.25%	1.75%	1.25%

The above Measurement Uncertainty values are the maximum amount of error for each axis expressed as a percentage of its full-scale load.

Calibration Temperature: 22.2°±1.1° C (72°±2° F)
 Temperature Compensation: hardware
 Calibration Method: WI-FTP-105, Net FT Calibration Instructions

Date of Calibration: 16 Dec 2020

Certificate Date: 16 Dec 2020
 Calibrated by: Mark Sinning, Calibration Technician

Engineered Products for Robotic Productivity

1031 Goodworth Drive, Apex, NC 27539, USA · Tel: +1.919.772.0115 · Fax: +1.919.772.8259 · www.ati-ia.com · E-mail: info@ati-ia.com

This certificate shall not be reproduced, except in full, without prior written approval from ATI. This certificate only applies to the items listed and does not include unlisted ancillary items such as data acquisition equipment. For questions or comments, please contact your ATI representative.

Certificate Number: FT32856-20201216

Page 1 of 6



Quality Statement

As part of our commitment to quality, each ATI force/torque transducer undergoes rigorous accuracy testing. This process, which involves applying and verifying a rich set of loading cases designed to cover the transducer's entire six-axis calibrated range, is designed to ensure that your transducer meets the measurement uncertainties listed in this Certificate of Calibration.

Our transducers often exceed our rigorous quality standards for accuracy. To ensure that the published transducer measurement uncertainties listed on page 1 are met, uncertainty targets used during the calibration process are more conservative than the published values. Often, transducers perform exceptionally well in certain loading situations. This report summarizes the performance of your ATI F/T transducer in our factory tests. It can be thought of as a 'best-case scenario' snapshot of your transducer's performance under laboratory conditions, in a variety of loading situations. You can expect the accuracy of your transducer measurements to fall somewhere between its performance during testing and the measurement uncertainties listed on its calibration certificate.

Certificate of Calibration

This calibration is traceable to the National Institute of Standards and Technology (NIST). ATI Industrial Automation (ATI) certifies that the listed product was calibrated in accordance with applicable ATI procedures. These procedures are compliant with the ISO 9001 standard to ensure that the listed product is within ATI's quality specifications. To meet this level of accuracy any loads must be correctly aligned to the transducer origin and the transducer must be robustly mounted to a surface of sufficient material strength and rigidity.

Note: If this is a recalibration of a legacy transducer that does not have precision locating features (such as dowel holes), users may experience additional error in measurements due to inexact mounting location. Precision locating features are highly recommended for best accuracy and can be added by ATI upon request.

The *Calibration Accuracy Section* contains several tables of data. The *Calibrated Ranges* (\pm) table lists the transducer's rated range for each axis. The *Applied Loads* table lists the loads applied during calibration and testing. The *Full-Scale Error* table shows the sensor system's measurement error as a percentage of full scale for each axis in each loading case. The *Offset Report* table, if included, shows transducer readings during offset adjustment and associated control limits. The *Gain-Check Report* table, if included, shows verification of the transducer's sensitivity and associated control limits. If included, the *Before and After Report* table shows a loading case relating the transducer's performance as received to its performance after recalibration.

For best accuracy, be sure to use your transducer's precision location features, and mount your transducer to a stiff surface. If an ongoing guarantee of sensor accuracy is important to you, we recommend that your sensor be tested annually. Contact your ATI Industrial Automation distributor to schedule recalibrations.

Engineered Products for Robotic Productivity

1031 Goodworth Drive, Apex, NC 27539, USA • Tel: +1.919.772.0115 • Fax: +1.919.772.8259 • www.ati-ia.com • E-mail: info@ati-ia.com

This certificate shall not be reproduced, except in full, without prior written approval from ATI. This certificate only applies to the items listed and does not include unlisted ancillary items such as data acquisition equipment. For questions or comments, please contact your ATI representative.

Certificate Number: FT32856-20201216

Page 2 of 6



Compliance Information - ISO 9001, A2LA, ANSI Z540, and ISO 17025

ATI Industrial Automation Inc. is an ISO 9001:2015 certified company. ATI's manufacturing facilities are not certified under A2LA, ANSI Z540, or ISO 17025, but our applicable processes are in compliance with these standards. As the designer and Original Equipment Manufacturer (OEM) of our Force/Torque Sensor products, we use validated, product-specific, proprietary manufacturing processes (including software), which no other facilities are capable of replicating. As the OEM of our Force/Torque Sensor products, ATI is not required to be A2LA, ANSI Z540, or ISO 17025 certified under the scope of our manufacturing operations. Parties interested in maintaining compliance with A2LA, ANSI Z540, or ISO 17025 standards as it pertains to their organization will find that our Force/Torque Sensor products meet several common exemption criteria specified in the aforementioned standards. In addition, 100% of our Force/Torque Sensor products are subjected to a testing and calibration sequence, specific to each sensor type, prior to shipping. When a part is returned as part of regularly scheduled maintenance (calibration) or a quality related-issue, it is re-processed through the same OEM testing and calibration sequence. All testing and calibration equipment used in our facilities are maintained in accordance with internal ISO 9001 compliant procedures and are traceable to NIST.

Engineered Products for Robotic Productivity

1031 Goodworth Drive, Apex, NC 27539, USA • Tel: +1.919.772.0115 • Fax: +1.919.772.8259 • www.ati-ia.com • E-mail: info@ati-ia.com

This certificate shall not be reproduced, except in full, without prior written approval from ATI. This certificate only applies to the items listed and does not include unlisted ancillary items such as data acquisition equipment. For questions or comments, please contact your ATI representative.

Certificate Number: FT32856-20201216

Page 3 of 6



Calibration Accuracy Section
Sensor System FT32856, Mini40/SI-80-4
Force units: N; Torque units: N-m

Calibrated Ranges (\pm)					
Fx	Fy	Fz	Tx	Ty	Tz
80	80	240	4	4	4

Applied Loads						
	Fx	Fy	Fz	Tx	Ty	Tz
1	0.000	33.362	0.000	-3.388	0.000	0.000
2	-33.362	0.000	0.000	0.000	-3.388	0.000
3	0.000	-33.362	0.000	3.388	0.000	0.000
4	33.362	0.000	0.000	0.000	3.388	0.000
5	0.000	71.172	0.000	-2.165	0.000	0.000
6	-71.172	0.000	0.000	0.000	-2.165	0.000
7	0.000	-71.172	0.000	2.165	0.000	0.000
8	71.172	0.000	0.000	0.000	2.165	0.000
9	0.000	28.913	0.000	-0.220	0.000	-3.307
10	0.000	28.913	0.000	-0.220	0.000	3.308
11	-28.913	0.000	0.000	0.000	-0.220	-3.306
12	-28.913	0.000	0.000	0.000	-0.220	3.306
13	0.000	-28.913	0.000	0.220	0.000	-3.308
14	0.000	-28.913	0.000	0.220	0.000	3.307
15	28.913	0.000	0.000	0.000	0.220	-3.306
16	28.913	0.000	0.000	0.000	0.220	3.306
17	0.000	0.000	44.482	-3.398	0.000	0.000
18	0.000	0.000	44.482	0.000	-3.397	0.000
19	0.000	0.000	44.482	3.384	0.000	0.000
20	0.000	0.000	44.482	0.000	3.396	0.000
21	0.000	0.000	177.929	0.000	0.000	0.000
22	0.000	0.000	-177.929	0.000	0.000	0.000
23	0.000	0.000	-44.482	3.398	0.000	0.000
24	0.000	0.000	-44.482	0.000	3.397	0.000
25	0.000	0.000	-44.482	-3.384	0.000	0.000
26	0.000	0.000	-44.482	0.000	-3.396	0.000

Refer to page 2 for important information on regarding this report.

Engineered Products for Robotic Productivity

1031 Goodworth Drive, Apex, NC 27539, USA · Tel: +1.919.772.0115 · Fax: +1.919.772.8259 · www.ati-ia.com · E-mail: info@ati-ia.com

This certificate shall not be reproduced, except in full, without prior written approval from ATI. This certificate only applies to the items listed and does not include unlisted ancillary items such as data acquisition equipment. For questions or comments, please contact your ATI representative.

Certificate Number: FT32856-20201216

Page 4 of 6



Full-Scale Error						
	Fx	Fy	Fz	Tx	Ty	Tz
1	0.43%	0.01%	-0.06%	0.17%	-0.51%	0.10%
2	-0.56%	0.00%	-0.11%	0.07%	0.64%	-0.15%
3	0.42%	-0.21%	-0.07%	-0.09%	-0.50%	-0.05%
4	-0.28%	-0.01%	0.03%	0.09%	0.17%	-0.04%
5	0.29%	0.36%	0.02%	0.04%	-0.34%	-0.32%
6	-0.66%	0.07%	0.11%	0.03%	0.22%	-0.23%
7	0.28%	-0.33%	0.05%	0.05%	-0.34%	-0.24%
8	-0.02%	0.08%	0.06%	0.05%	0.17%	-0.25%
9	-0.05%	-0.36%	0.03%	-0.30%	0.09%	0.15%
10	-0.15%	-0.56%	0.02%	0.07%	-0.08%	0.04%
11	0.31%	0.06%	0.04%	-0.17%	-0.16%	-0.01%
12	0.37%	0.02%	0.05%	0.19%	-0.16%	0.10%
13	-0.15%	0.63%	0.00%	0.19%	-0.23%	0.08%
14	-0.02%	0.46%	0.01%	-0.13%	0.23%	0.08%
15	-0.61%	-0.16%	0.02%	0.18%	0.36%	0.00%
16	-0.70%	0.25%	0.02%	-0.23%	0.07%	0.00%
17	0.35%	0.01%	-0.29%	0.30%	-0.64%	-0.12%
18	-0.24%	0.12%	-0.22%	0.18%	0.61%	0.23%
19	0.33%	0.07%	-0.27%	0.07%	-0.66%	-0.06%
20	-0.40%	0.08%	-0.31%	0.06%	0.51%	-0.13%
21	-0.10%	0.38%	0.13%	0.00%	-0.31%	-0.04%
22	-0.08%	0.29%	-0.19%	0.13%	-0.27%	-0.04%
23	0.32%	0.37%	0.01%	0.15%	-0.35%	0.02%
24	-0.52%	0.20%	0.05%	0.17%	0.45%	0.10%
25	0.28%	-0.10%	0.04%	-0.31%	-0.36%	-0.02%
26	-0.15%	0.15%	0.08%	0.09%	-0.06%	-0.17%

Refer to page 2 for important information on regarding this report.

Offset Report						
	Fx	Fy	Fz	Tx	Ty	Tz
F/T Offset	-0.0001	-0.0028	-0.0028	-0.0002	0.0001	0.0001
	SG0	SG1	SG2	SG3	SG4	SG5
SG Offset	0.5650	0.1000	0.8850	0.7850	0.9650	0.7500
±SG Limit	1599.9638	1599.9638	1599.9638	1599.9638	1599.9638	1599.9638

Offsets are measured in a unique configuration not available to the user.
Refer to page 2 for important information on regarding this report.

Engineered Products for Robotic Productivity

1031 Goodworth Drive, Apex, NC 27539, USA · Tel: +1.919.772.0115 · Fax: +1.919.772.8259 · www.atl-ia.com · E-mail: info@atl-ia.com

This certificate shall not be reproduced, except in full, without prior written approval from ATI. This certificate only applies to the items listed and does not include unlisted ancillary items such as data acquisition equipment. For questions or comments, please contact your ATI representative.

Certificate Number: FT32856-20201216

Page 5 of 6



Gain-Check Report						
	SG0	SG1	SG2	SG3	SG4	SG5
Lower Limit	0.8000	0.8000	0.8000	0.8000	0.8000	0.8000
Lower Output	0.9123	0.8770	0.8974	0.9118	0.8998	0.9120
Upper Output	0.9273	0.8832	0.9123	0.9134	0.9113	0.9135
Upper Limit	1.0000	1.0000	1.0000	1.0000	1.0000	1.0000

Gain readings are measured in a unique loading configuration.

Engineered Products for Robotic Productivity

1031 Goodworth Drive, Apex, NC 27539, USA · Tel: +1.919.772.0115 · Fax: +1.919.772.8259 · www.ati-ia.com · E-mail: info@ati-ia.com

This certificate shall not be reproduced, except in full, without prior written approval from ATI. This certificate only applies to the items listed and does not include unlisted ancillary items such as data acquisition equipment. For questions or comments, please contact your ATI representative.

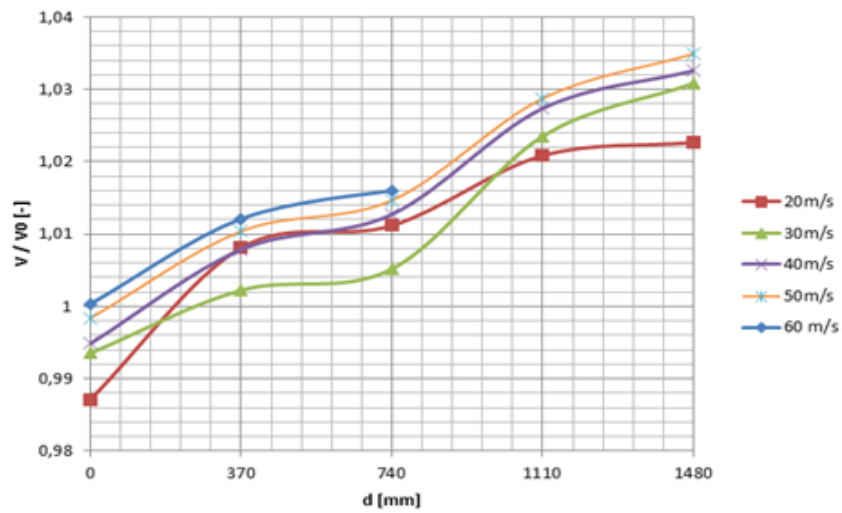
Certificate Number: FT32856-20201216

Page 6 of 6

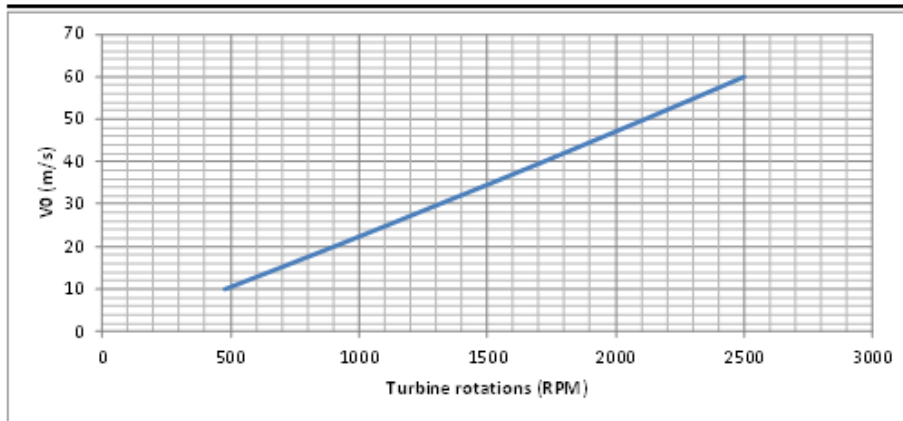
Longitudinal velocity distribution

Date:	19-5-2021	Module:	Free flow characteristics
Ambient temperature:	22,016 C	Technician	Hendrik de Boer
Section pressure	PX 655 10D1	Ambient pressure	97617,437 Pa
Reference pressure	PX 655 25BDI		

Description: Pressure measurements at various lengths along the test section
 Pressure is compared to the inlet pressure at distance 0

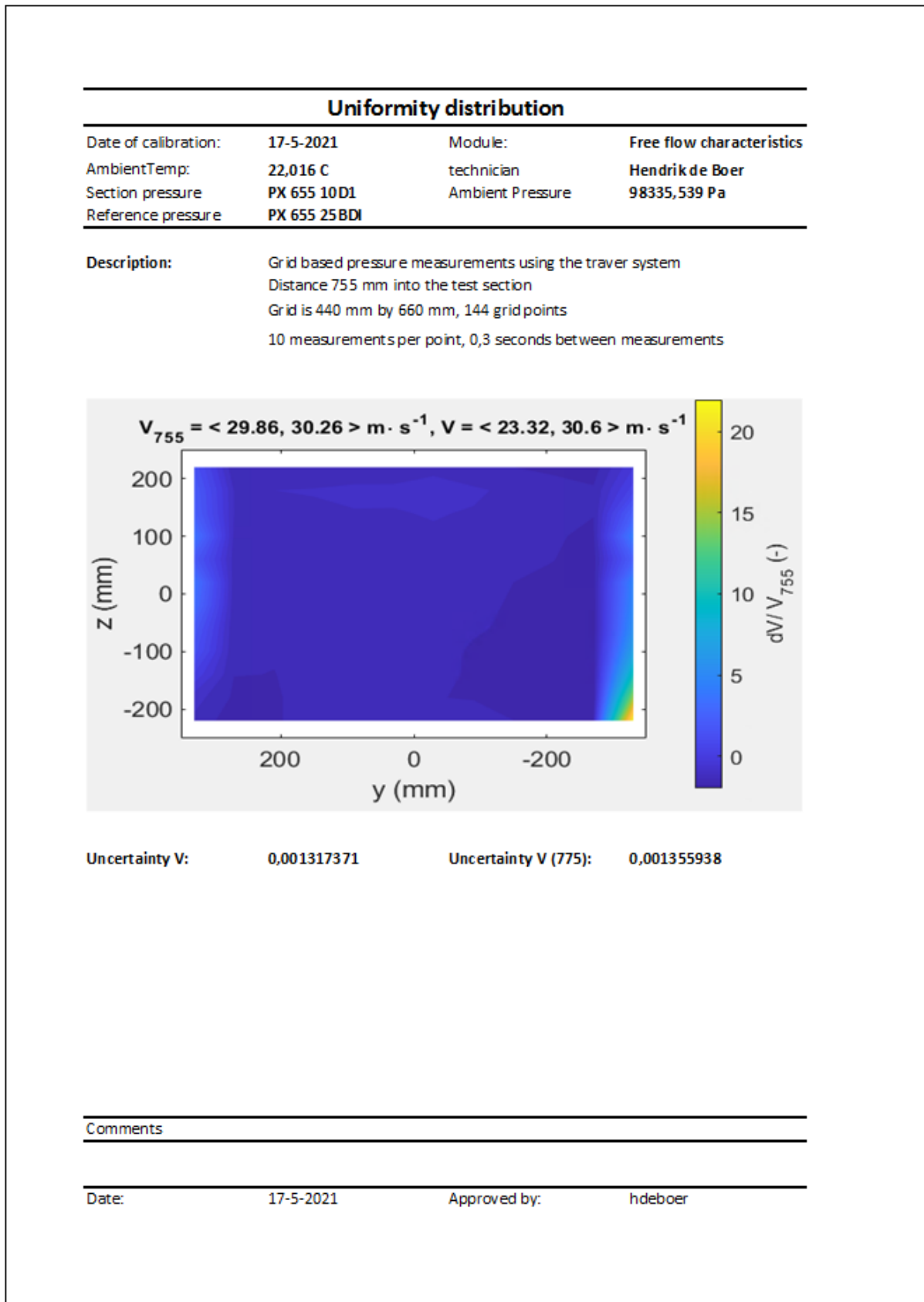


RPM for V0



Comments

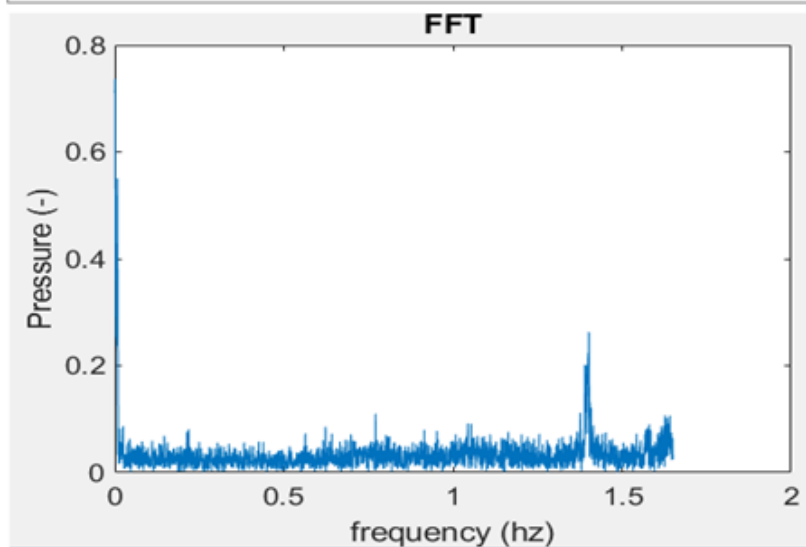
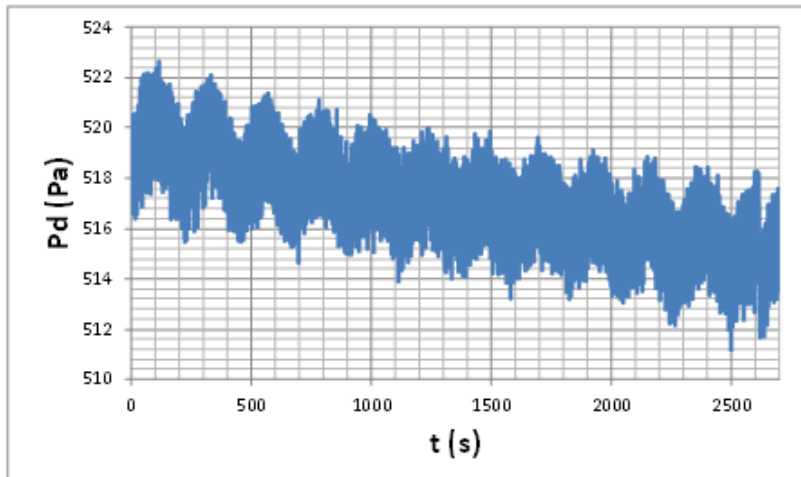
Date: 19-5-2021 Approved by: hdboyer



Large scale fluctuations

Date of Calibration:	17-5-2021	Module:	Free flow characteristics
AmbientTemp:	22,016 C	Technician:	Hendrik de Boer
Measurement device:	PX 655 25BDI	Ambient Pressure:	97667,703

Description: Static pressure measured over the span of the 40 minutes
 Stable turbine rotations per minute during the time span
 Fourier transform made of the static pressure over time



Comments

Fluctuations are ever present, but different per experiment. PID controller needs to be checked. Otherwise keep track of the fluctuations in both V0 and V measurements

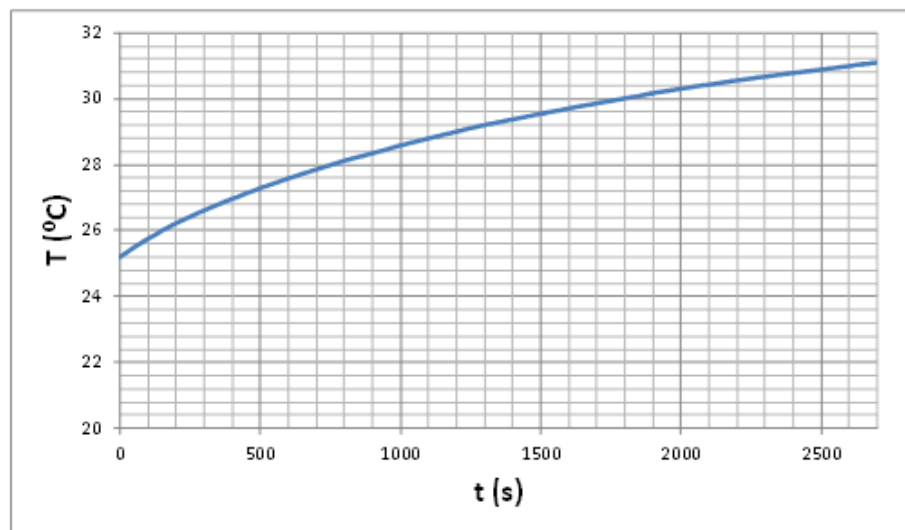
Date: 17-5-2021 Approved by: hdeboer

Calibration Report

Date of Calibration:	17-5-2021	Module:	Free flow characteristics
AmbientTemp:	22,016 C	Technician:	Hendrik de Boer
Measurement device:	Type K thermocouple	Ambient Pressure:	97667,703

Description: Temperature of inside the tunnel measured over 40 minutes
 Average of two thermocouples is used
 Stable turbine rotations per minute during the time span

Flow temperature over time



$$T = -6 \times 10^{-7} t^2 + 0,0036t + 25,551$$

Comments

Given equation for the temperature is an estimation, and depends on the circumstances

Date: 17-5-2021 Approved by: hdeboer